Journal of Environmental Chemical Engineering 13 (2025) 115559

Contents lists available at ScienceDirect

Journal of Environmental Chemical Engineering

journal homepage: www.elsevier.com/locate/jece

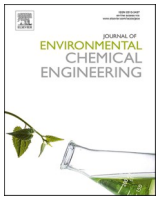

Investigation of product properties and reaction mechanism of low-rank coal pyrolysis with phosphorite in a fluidized bed

Zhihua Tian [a,1], Bin Zhang [a,1], Qinhui Wang [a,*], Qigang Deng [b], Guohui Xu [b], Ruiqing Jia [a], Dong Ma [a], Yingchi Chen [a]

[a] State Key Laboratory of Clean Energy Utilization, Zhejiang University, Hangzhou 310027, China
[b] Dongfang Electric Corporation - Zhejiang University Joint Innovation Research Institute, Hangzhou, China

ARTICLE INFO

Keywords:
Fluidized bed
Low-rank coal
Pyrolysis products
Migration of Na and Cl
Waste recycling

ABSTRACT

This study investigates the co-pyrolysis of low-rank, high-alkaline coal with phosphorite to enhance resource utilization and mitigate equipment corrosion caused by alkali metal emissions during the thermal processing of high-sodium coal. Pyrolysis experiments were conducted in a fluidized bed reactor, with different temperature and phosphorite ratios. The results demonstrate that the interaction between phosphorite and coal macromolecules can promote the decomposition of aromatic compounds. At 700 °C, after adding 15 % phosphorite, the yields of char and gas of Naomaohu coal (NM coal) increased by 3.14 % and 0.65 %, and the yield of tar decreased by 5.29 %. Meanwhile, compounds such as calcium, aluminum, and silicon contained in phosphorite react with Na and Cl to inhibit the release of corrosive substances. At 900 °C, after adding 15 % phosphorite, the release ratios of Na and Cl decreased by 15.67 % and 16.05 %, respectively. The changes in the pyrolysis products of Hami coal (HM coal) are consistent with those of NM coal. Calcium fluorophosphate and calcium phosphate in phosphorite can react with alkali metal chlorides and sulfides to form phosphates that are more easily reduced. The use of recycled phosphorite enhances both the conversion ratio and product quality in yellow phosphorus production. This method not only improves the quality of pyrolysis products but also optimizes the thermal utilization of high-alkali coal and phosphorite, providing a cost-effective and efficient approach for resource utilization.

1. Introduction

With ongoing economic development and population growth, global energy demand is rising sharply. Coal, with its abundant reserves in China, remains pivotal for ensuring energy security [1,2]. Pyrolysis technology stands out as a crucial method for the efficient and environmentally friendly utilization of coal resources, offering high resource utilization efficiency and economic viability [3–6]. Post pyrolysis, products such as char, tar, and syngas are obtained, which find diverse industrial applications based on their properties [7,8]. In China, the Zhundong and Hami regions of Xinjiang hold significant low-rank, high-alkaline coal reserves, accounting for 17.7 % of the country's predicted coal reserves [9]. Low-grade and high-alkali coal will release a large amount of greenhouse gas CO_2 and corrosive substances such as NaCl during its utilization, which will cause serious pollution to the environment [10–12]. Enhancing the utilization efficiency of these coal resources and mitigating the release of corrosive substances during thermal utilization are critical research areas [13–15]. Investigating the pyrolysis mechanisms, optimizing conditions, and enhancing product quality are paramount for industrial efficiency and cost-effectiveness.

At present, many scholars have explored different coal pyrolysis technologies [16] and various factors affecting coal pyrolysis [17], including temperature [18], heating rate [19], pressure [20], coal type [21], and particle size [22]. Some scholars have studied the pyrolysis mechanism of low-rank coal [23–25], and some scholars have also made significant discoveries in the study of adding external additives during the pyrolysis process [26]. Öztaş and Yürüm [27] demonstrated that metal compounds containing Mg, Ca, and Fe can enhance coal pyrolysis conversion ratios. Yang and Cai [28] discovered that adding transition metal catalysts enhances char reactivity. Franklin et al. [29] reported that CaO suppresses tar production and catalyzes the cracking of functional groups and aromatic components. Wu et al. [30] investigated the

* Correspondence to: Zhejiang University, Lingyin Street, Xihu District, Hangzhou, Zhejiang, China.
E-mail address: qhwang@zju.edu.cn (Q. Wang).
[1] These authors contributed equally to this work.

https://doi.org/10.1016/j.jece.2025.115559
Received 13 September 2024; Received in revised form 3 December 2024; Accepted 21 January 2025
Available online 25 January 2025

effects of $CaCl_2$ on fine particle formation during pyrolysis. Franklin et al. [31] and Murakami et al. [32] found that CaO or $CaCO_3$ reduces tar and hydrocarbon yields, with CaO having a greater catalytic effect on aromatic components. Despite these advances, most studies have used pure compounds such as $CaCl_2$, CaO, $CaCO_3$, MgO as additives for experiments, and few studies have used natural minerals. The high cost of these pure compounds limits their industrial applicability and scalability. Moreover, the treatment of these pure compounds after pyrolysis is also a serious issue. The selection of additives with easier post-treatment processes is the focus of this study. In addition, most studies have used fixed bed reactors, and fewer studies have used fluidized bed reactors. Therefore, this study used a fluidized bed reactor and selected phosphorite, a natural calcium-containing mineral with a lower cost, as the additive. This study mainly studies the effect of phosphorite on the pyrolysis of high-alkali low-rank coal, and explores the changes in its product characteristics and the release of Na and Cl. This can provide a new method to improve product quality and reduce the cost of coal pyrolysis process.

China, holding 3.22 billion tons of phosphorite resources, ranks second and is the largest producer globally [33]. Only 7 % of these reserves are high-grade (P_2O_5 content >30 %), while 80 % are medium-grade and low-grade (P_2O_5 content <25 %) [34]. The thermal-process method is the main process for yellow phosphorus production due to its applicability for various grades of phosphorite, though it has a low conversion ratio and high cost [35–38]. Improving the conversion ratio and reducing the production cost of thermal-process phosphoric acid are urgent issues that need addressing. Phosphorite contains substantial calcium-based components, Al_2O_3, and SiO_2, which can participate in coal pyrolysis and affect the products [39]. These components facilitate higher yields of char and pyrolysis gas while reducing emissions of alkali metal chlorides and sulfides, improving boiler operation safety.

In summary, this study provides a new method to maximize the utilization of phosphorite and low-rank high-alkali coal. Phosphorite is abundant in Guizhou, Yunnan, and Xinjiang province, and has low mining and transportation costs compared to other calcium-containing additives. Although high-alkali low-rank coal is abundant and low-cost, it faces limitations due to its high sodium and chlorine content, which leads to equipment corrosion. Co-pyrolysis of phosphorite and low-rank high-alkali coal can improve the quality and value of pyrolysis products, reduce Na and Cl emissions, and reduce equipment maintenance costs. In addition, phosphorite can be recycled for phosphoric acid production, thereby reducing post-processing costs and improving the conversion ratio of phosphorite. This method is both economically feasible and sustainable, and has strong potential for industrial application.

2. Experimental method

2.1. Pyrolysis experiments

This study investigated the effects of phosphorite on pyrolysis products using Hami coal (HM coal) and Naomaohu coal (NM coal) from Xinjiang A fluidized bed reactor with 99 % pure quartz sand as the bed material was utilized. The coal, phosphorite, and quartz sand were dried at 105 ± 5 °C for 12 hours and then sieved: coal (0.900–2.50 mm), phosphorite (0.425–0.700 mm), and quartz sand (0.250–0.350 mm). The samples were ashed according to GB/T 212–2008. The ash composition of phosphorite and the two types of coal are shown in Table 1, while Table 2 presents the proximate and ultimate analysis.

The pyrolysis experiments were conducted on a small-scale bubbling fluidized bed reactor (Fig. 1), constructed entirely of 310 s stainless steel and capable of heating up to 1000 °C. This equipment includes the fluidized bed reactor body, an air supply system, a screw feeder, a cyclone separator, a tar condensation and collection system, a gas collection system, and a control system. The reactor has an internal diameter of 30 mm and a height of 700 mm, with a 5.5 m long preheating section. Three pressure measurement points and five thermocouple sheaths provide real-time monitoring of pressure and temperature.

During pyrolysis, the temperature in the fluidized bed reactor remains uniform, with a difference within 20 °C across different regions. Ar was selected as the pyrolysis atmosphere. 150 g of quartz sand was fed through the top inlet, while 15 g of coal was introduced through a side-mounted screw feeder, cooled by circulating water to prevent premature pyrolysis. The particle size of the selected quartz sand ranges from 0.25 to 0.35 mm, with a corresponding static bed height of 143.90 mm for 150 g of quartz sand. The measured critical fluidization carrier gas flow rate is 3.0 L/min. To ensure complete fluidization of the material, facilitate the full collection of tar, and maintain the gas volume within the collection range of the gas collection bag, the carrier gas flow rate is set at 1.3–1.5 times the critical fluidization flow rate, resulting in a selected flow rate of 4.2 L/min [40–42]. Preliminary experiments have shown that the yields of the four products still vary before 20 minutes of pyrolysis, but their yields vary very little after 20 minutes. Therefore, the pyrolysis time was selected to be 20 minutes. Tar and pyrolysis water were collected using a serpentine quartz glass tube in an alcohol thermostatic bath at −40 °C. Pyrolysis gas was collected in gas bags for subsequent analysis. After the reaction, the bottom carbon hopper was opened to collect the resulting char and bed material, which were allowed to cool before being discharged to avoid oxidation by air. In industrial production, 500–900 °C is a common temperature range for low-rank coal pyrolysis. This is based on the precipitation characteristics of tar and volatile matter at different temperatures. 500 °C is the temperature at which the coal pyrolysis reaction begins to occur violently. At this temperature the volatile matter in the coal begins to be released. As the temperature increases, the distribution of tar, gas and char changes significantly. 900 °C is the upper limit of the high-temperature pyrolysis process. At this temperature, the volatile matter is basically completely released, the solid carbon gradually becomes stable, and the pyrolysis reaction proceeds almost completely. There is little point in raising the temperature any further. Therefore, the temperature range of 500–900 °C was selected to comprehensively investigate the evolution and characteristics of the products during the pyrolysis process.

The solid products were cooled to room temperature, discharged from the air-isolated hopper, and sieved (0.700 mm and 0.350 mm) to separate char from co-pyrolyzed phosphorite. The char was weighed to determine its mass (M_{char}). The range of the balance used in this experiment is 0–120 g, which can be accurate to 0.0001 g. When repeatedly weighing the same sample, the relative standard deviation can usually be kept below 0.01 %. The pyrolysis gas was analyzed using a gas chromatograph, with its volume calculated using the argon tracer method. Eq. (1) was used to calculate the mass of the pyrolysis gas (M_{gas}).

Table 1
Ash composition of coal and phosphorite.

Sample	Composition	SiO_2	Al_2O_3	Fe_2O_3	CaO	MgO	K_2O	Na_2O	P_2O_5
NM coal	wt%	38.79	9.21	7.35	25.81	4.22	0.45	4.90	~
HM coal	wt%	19.44	13.20	12.89	31.04	3.72	0.23	5.63	~
Phosphorite	wt%	36.42	7.7	1.19	23.1	5.27	0.86	0.16	21.53

Table 2
Proximate analysis and ultimate analysis of coal.

Sample	Industrial analysis w/%				Elemental analysis w/%					Calorific value(J·g^{-1})
	M_{ad}	A_{ad}	V_{ad}	FC_{ad}	C_{ad}	H_{ad}	N_{ad}	S_{ad}	O_{ad}	
NM coal	6.18	11.32	31.46	50.92	60.61	3.78	0.95	0.24	16.27	22436
HM coal	4.50	6.91	36.03	52.56	67.87	4.46	1.06	0.30	14.90	26763

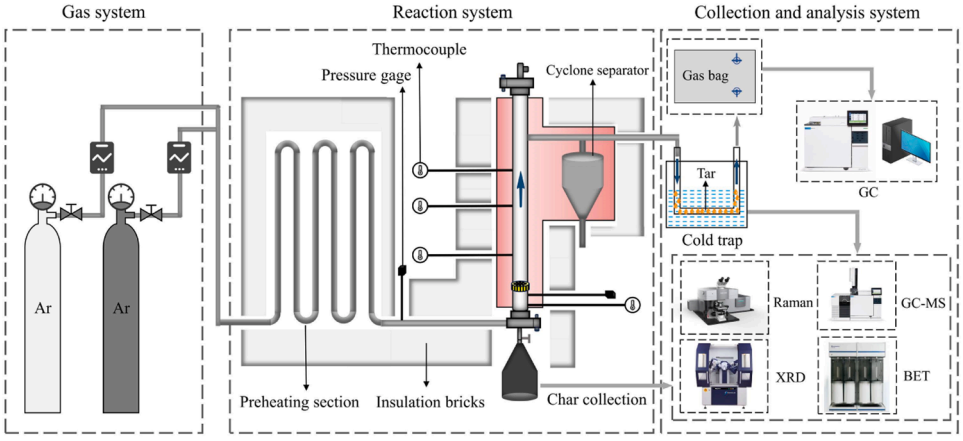

Fig. 1. A fluidized bed reactor.

$$M_{gas} = \frac{M_{Ar}}{N_{Ar}} \cdot \left(1 - N_{Ar}\right) = \frac{V_{Ar} \cdot t \cdot c \cdot M_r}{V_m \cdot N_{Ar}} \cdot \left(1 - N_{Ar}\right) \quad (1)$$

In the **Equation**, V_{Ar} is the volume of Ar (L), N_{Ar} is the mass fraction of Ar, t is the pyrolysis time (min), c is the inflow rate (L•min^{-1}), V_m is the molar volume at standard conditions (22.4 L•mol^{-1}), M_r is the relative atomic mass of Ar (40 g•mol^{-1}). The contents of CO, CO_2, CH_4, and H_2 were determined by multiplying the gas mass by the mass fractions measured by the gas chromatograph. In this experiment, the Agilent 8860 gas chromatograph was used to measure the gas product components. In the repeatability test, the device showed a low relative standard deviation (usually within the range of ± 1–2 %), ensuring the consistency and reliability of the analysis results.

The liquid condensation and collection system, consisting of a quartz serpentine condenser, gasoline filter core, glass fiber filter cartridge, and connecting ducts, was weighed before and after the experiment to determine the total mass of the mixed liquid (M_a). The system was rinsed with pure acetone, and the liquid was collected and weighed (M_{liquid}). The water content (a) was determined using an SF-5 type coulometric Karl Fischer moisture meter and the mass of pyrolysis water (M_{water}) was calculated using Eq. (2). The mass of tar (M_{tar}) was determined by the difference method shown in Eq. (3). The SF-5 type coulometric Karl Fischer moisture meter can achieve a moisture measurement accuracy of ± 0.1 % under standard conditions. Through repeatability experiments, it was found that its standard deviation is usually between 0.01 % and 0.03 %.

$$M_{water} = M_{liquid} \cdot a \quad (2)$$

$$M_{tar} = M_a - M_{water} \quad (3)$$

The yields of char, tar, pyrolysis water, and pyrolysis gas for each sample are calculated by dividing their mass by the initial coal mass. The collected char was ground to below 200 mesh. A 0.1 g sample was digested, and diluted to 100 mL, and the sodium content (n_1, g•g^{-1}) was determined using ion chromatography. The total sodium content in the char was then calculated. The content of chloride in the char was determined using the silver nitrate titration method with potassium thiocyanate solution, as specified in GB/T 3558–1996. The release ratios of Na (η_{Na}) and Cl (η_{Cl}) during pyrolysis were calculated using Equation (4) and Eq. (5).

$$\eta_{Na} = \frac{n_1 \cdot m_{char}}{n_{Na} \cdot m_{coal}} \quad (4)$$

$$\eta_{Cl} = \frac{n_1 \cdot m_{char}}{n_{Cl} \cdot m_{coal}} \quad (5)$$

In the Equations, n_{Na} (g•g^{-1}) and n_{Cl} (g•g^{-1}) represent the relative content of sodium and chlorine in the coal, m_{char} (g) is the mass of char, and m_{coal} (g) is the mass of coal.

2.2. Phosphorite reduction experiments

Phosphorite reduction was conducted using a thermal reduction process in a fixed bed reactor that can be heated up to 1400 °C. The co-pyrolyzed phosphorite was ground to below 0.150 mm. Based on previous studies [33,35,43], 5 g of phosphorite was weighed for each experiment, with carbon and high-purity SiO_2 added according to the P_2O_5 content of the phosphorite. The carbon excess coefficient was 1.6 and the silicon-calcium molar ratio was 2.0. The reactor was heated at 10 °C/min, and nitrogen gas was introduced at a flow rate of 500 L/h. Samples were thoroughly mixed and introduced for reaction once the reactor reached the set temperature. After the reaction, the reactor cooled naturally, and the residual slag was collected and weighed. The P_2O_5 content in the residue was determined using GB/T 1871.1–1995. The phosphorite conversion ratio was calculated using Eq. (6).

$$\eta = \frac{m_1 x_1 - m_2 x_2}{m_1 x_1} \times 100\% \quad (6)$$

In the Equation, η (%) is the conversion ratio of phosphorite, x_1 (%) is the mass fraction of P_2O_5 in the phosphorite, x_2 (%) is the mass fraction of P_2O_5 in the residue. m_1 (g) is the mass of phosphorite, m_2 (g) is the mass of the slag.

3. Results and discussion

3.1. Kinetic analysis of co-pyrolysis with phosphorite

For the kinetic analysis of co-pyrolysis, an automatic simultaneous

thermal analysis system (TGA/DSC 3 +) was used. This system operated at a heating rate of 10 °C/min under a nitrogen flow rate of 50 mL/min, increasing the temperature from room temperature to 1000 °C. Mixtures of two types of coal with varying amounts of phosphorite were prepared in the following ratios (coal to phosphorite): 100:0, 100:3, 100:6, 100:9, 100:12, and 100:15. Each mixture (10 mg) was used for each ratio, ensuring a consistent mass of coal per experiment. Approximately 1 g of three different phosphorite samples were heated in a fixed bed under a nitrogen atmosphere up to 1000 °C. The phosphorite samples showed negligible weight loss, all less than 1.5 %, which was disregarded in the calculation of the thermogravimetric curves due to their minimal contribution.

Fig. 2 shows the pyrolysis TG-DTG curve of the samples. The weight on the thermogravimetric curve indicates the mass of the coal, and the mass of phosphorite has been subtracted. Fig. 2(a) and (c) depict the TG curves of NM coal and HM coal, respectively, where the process before 100 °C primarily involves the removal of moisture from the coal. Fig. 2 (b) and (d) show the corresponding DTG curves for NM coal and HM coal. From these figures, it is evident that the TG and DTG curves exhibit similar trends for both types of coal. Regardless of the presence of

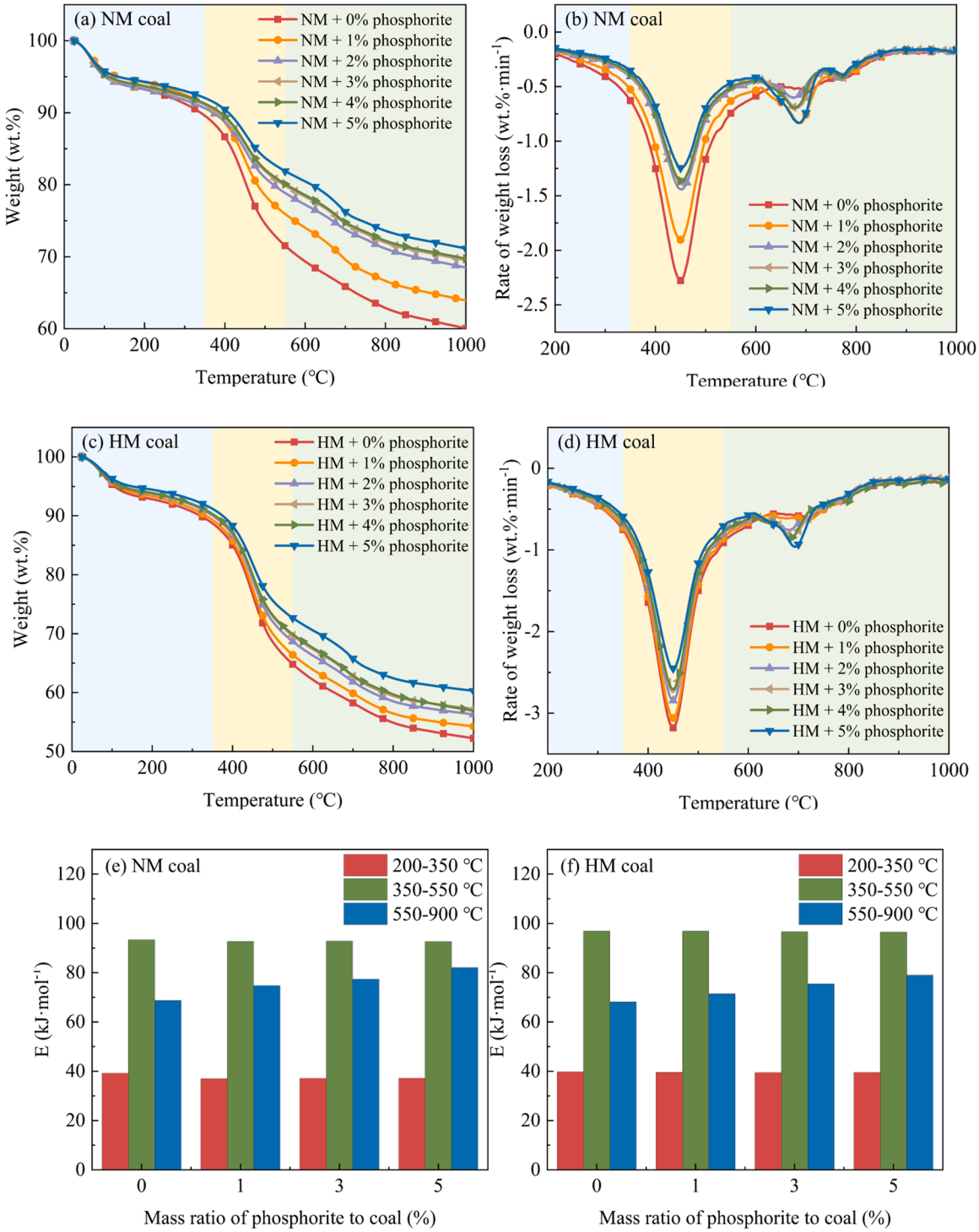

Fig. 2. TG-DTG curves of coal co-pyrolyzed with phosphorite.

phosphorite during pyrolysis, the coal decomposition process can be divided into three stages. In the temperature range from room temperature to 350 °C, there is minimal weight loss, indicative of desorption processes involving weak molecular bonds and adsorbed gases from pores. During this phase, gases such as CH_4, CO_2, and CO are released. Between 350 °C and 550 °C, the TG curve shows a significant decrease, with a corresponding peak in the DTG curve around 450 °C. This signifies deeper pyrolysis reactions with faster reaction rates, resulting in a substantial generation of pyrolysis gases and tar. It can also be seen from Fig. 2 that different phosphorite addition ratios have a significant effect on the pyrolysis weight loss process of low-rank coal. The maximum weight loss rate of NM coal and HM coal pyrolysis process occurs in the range of 400–500 °C. With the increase of phosphorite addition ratio, the weight loss of coal pyrolysis decreases slightly, and the maximum weight loss rate gradually decreases. This effect is attributed to the presence of calcium-based compounds in phosphorite [44], where Ca acts as cross-linking points within the coal's macromolecular structure, hindering the decomposition of char into smaller molecular tar components [45,46]. At temperatures exceeding 550 °C, the TG curve continues to decline, while the DTG curve flattens out, indicating predominant cross-linking reactions and condensation processes of char. Around 690 °C, a peak appears in the DTG curve due to intermolecular reactions of functional groups within coal, leading to the release of small molecular gases such as H_2 and CO. This peak is more pronounced when phosphorite is added, as calcium compounds react with carboxyl and hydroxyl groups in coal, releasing volatile components such as CO_2 and H_2O [47]. Upon heating, calcium fluorapatite in phosphorite reacts with SiO_2 to produce significant amounts of CaO and $CaCO_3$, enhancing the release of gases during coal pyrolysis around 690 °C and thereby amplifying the reduction in weight loss observed in the TG curve.

The reactions involved in these processes are represented by (R1–8). A detailed analysis of the TG and DTG curves reveals the thermal decomposition behaviors of NM coal and HM coal, emphasizing the role of phosphorite in influencing the kinetics and mechanisms of coal pyrolysis.

$$4Ca_5(PO_4)_3F + SiO_2 \rightarrow 6Ca_3(PO_4)_2 + SiF_4 + 2CaO \quad \text{(R1)}$$

$$CaO + CO_2 \rightarrow CaCO_3 \quad \text{(R2)}$$

$$\text{R-OH} + CaCO_3 + \text{R'-OH} \rightarrow \text{R-O-Ca-O-R'} + CO_2 + H_2O \quad \text{(R3)}$$

$$\text{R-O-Ca-O-R'} + CO_2 \rightarrow \text{R-O-R'} + CaCO_3 \quad \text{(R4)}$$

$$\text{R-COOH} + CaCO_3 + \text{R'-COOH} \rightarrow \text{R-COO-Ca-COO-R'} + CO_2 + H_2O \quad \text{(R5)}$$

$$\text{R-COO-Ca-COO-R'} \rightarrow \text{R-CO-R'} + CaCO_3 \quad \text{(R6)}$$

$$\text{R-COOH} + CaCO_3 + \text{R'-OH} \rightarrow \text{R-COO-Ca-O-R'} + CO_2 + H_2O \quad \text{(R7)}$$

$$\text{R-COO-Ca-O-R'} + CO_2 \rightarrow \text{R-COO-R'} + CaCO_3 \quad \text{(R8)}$$

Coal pyrolysis involves multiple parallel and competing reactions internally. Conducting kinetic analysis of coal pyrolysis helps in understanding the process, calculating reaction rates, and assessing the difficulty of various reactions [48]. Based on different temperature ranges and their characteristics, coal pyrolysis can be divided into stages including drying and degassing, intense pyrolysis, and char consolidation [49,50]. This study categorizes the pyrolysis process into three stages: 200 °C to 350 °C, 350 °C to 550 °C, and 550 °C to 900 °C. To better reflect the characteristics of pyrolysis reactions within each stage, kinetic analysis was conducted in each temperature range and the main kinetic parameters were calculated.

$$\alpha = \frac{m_0 - m_1}{m_1 - m_\infty} \quad (7)$$

$$\frac{d\alpha}{dt} = A(1-\alpha)^n \cdot \exp\left(-\frac{E}{RT}\right) \quad (8)$$

$$\ln\left[1 - \frac{(1-\alpha)^{(1-n)}}{T^2(1-n)}\right] = \ln\left[\frac{AR}{\beta E}\left(1 - \frac{2RT}{E}\right)\right] - \frac{E}{RT} \quad (9)$$

$$\ln\left[\frac{-\ln(1-\alpha)}{T^2}\right] = \ln\left[\frac{AR}{\beta E}\left(1 - \frac{2RT}{E}\right)\right] - \frac{E}{RT} \quad (10)$$

This study employed the widely used Coast-Redfern integral method [51] for kinetic analysis. This method utilizes a single scan rate approach, primarily for the kinetic analysis of samples under constant heating rate conditions in thermogravimetric experiments [52]. During the thermal reaction process, the initial mass of the sample is m_0, the mass at a given time is m_1, and the final mass after the reaction is m_∞. The mass conversion ratio α at that time can be calculated using Eq. (7). According to the Arrhenius equation, the reaction rate of coal pyrolysis, $d\alpha/dt$, is expressed by Eq. (8), where E (kJ·mol^{-1}) denotes the activation energy, T (K) is the temperature, and R (8.314 J•mol^{-1}•K^{-1}) is the universal gas constant. By substituting the program heating rate $\beta = dT/dt$ into Eq. (8) and integrating concerning temperature using a first-order approximation, and considering that E/RT is significantly greater than 1, the simplified equations derived are shown in Eq. (9) and Eq. (10). Eq. (9) is applied to calculate the reaction order $n \neq 1$, while Eq. (10) is used for $n = 1$ reactions. Previous studies [53,54] have indicated that coal pyrolysis typically exhibits first-order kinetics ($n = 1$). Therefore, plotting $1/T$ as the x-axis and $\ln[-\ln(1-\alpha)/T^2]$ as the y-axis, fitting the data points yields a straight line. The slope of this line provides $-E/R$ and the intercept provides $\ln(AR/\beta E)$. These fitted parameters enable the calculation of the activation energy E (kJ·mol^{-1}) and the pre-exponential factor A (min^{-1}). The calculated results are presented in Table 3.

From Table 3, it is evident that the trends in activation energy during the pyrolysis process of NM coal and HM coal are similar. The temperature ranges of 200–350 °C, 350–550 °C, and 550–900 °C correspond to the first, second, and third stages of pyrolysis, respectively. Both coals exhibit apparent activation energies between 35 and 100 kJ·mol^{-1}. As organic matter begins to participate in pyrolysis [55], the increase in reaction temperature from the first stage to the second stage leads to an increase in activation energy. For NM coal, the activation energy increases from 39.20 kJ·mol^{-1} to 93.40 kJ·mol^{-1}, while for HM coal, it increases from 39.78 kJ·mol^{-1} to 96.86 kJ·mol^{-1}. The carbon on the surface of both coals undergoes gas-solid reactions with CO_2 generated during pyrolysis at high temperatures. This reaction rate increases significantly at higher temperatures, transitioning from kinetic control to diffusion control in the third stage [56], thereby resulting in lower activation energies in the third stage compared to the second stage. According to Table 3, the activation energy for NM coal decreases from 93.40 kJ·mol^{-1} to 68.71 kJ·mol^{-1}, whereas for HM coal, it changes from 96.86 kJ·mol^{-1} to 68.12 kJ·mol^{-1}.

Upon adding phosphorite to the samples, it was observed that phosphorite has a similar effect on the pyrolysis of both coals. The addition of phosphorite slightly lowers the activation energies of the first and second stages of pyrolysis for NM coal. Specifically, adding 15 % phosphorite relative to the coal mass decreases the activation energy of the first stage by 1.98 kJ·mol^{-1}, and the second stage by 0.74 kJ·mol^{-1} for NM coal. However, phosphorite has minimal impact on the first and second stages of pyrolysis for HM coal, with activation energies decreasing by only 0.22 kJ·mol^{-1} and 0.34 kJ·mol^{-1}, respectively. During the pyrolysis of both coals, phosphorite significantly affects the third stage. Adding 15 % phosphorite increases the activation energy of the third stage by 13.43 kJ·mol^{-1} for NM coal and by 10.90 kJ·mol^{-1} for HM coal, indicating that phosphorite addition inhibits the third-stage pyrolysis reactions. This results in some large molecular groups that would normally decompose into tar and carbon on the coal surface being oxidized by H_2O and CO_2, reducing the release of volatile components and thereby increasing the yield of char. This observation aligns with the trend observed in Fig. 2, where the final mass of samples with added phosphorite is higher than that of samples

Table 3
Kinetic parameters of co-pyrolysis of coal and phosphorite at 10 K/min.

Type of coal	Temperature Range (℃)	Mass ratio of phosphorite to coal (%)	Linear Fitting Equation	E (kJ·mol^{-1})	A (min^{-1})	r^2
NM coal	200–350	0	y = −4714.42x−4.49	39.20	13.19	0.987
		1	y = −4450.35x−4.85	37.00	8.683	0.982
		3	y = −4464.63x−4.83	37.12	8.931	0.982
		5	y = −4477.25x−4.80	37.22	9.185	0.983
	350–550	0	y = −11233.6x+ 1.85	93.40	442.1	0.979
		1	y = −11149.7x+ 1.70	92.70	507.4	0.981
		3	y = −11165.5x+ 1.72	92.83	498.7	0.981
		5	y = −11144.7x+ 1.69	92.66	512.4	0.981
	550–900	0	y = −8264.72x−5.59	68.71	7.755	0.961
		1	y = −8988.70x−4.92	74.73	16.35	0.961
		3	y = −9307.84x−4.59	77.39	23.62	0.957
		5	y = −9879.45x−4.03	82.14	44.01	0.954
HM coal	200–350	0	y = −4785.02x−4.59	39.78	11.85	0.987
		1	y = −4767.32x−4.45	39.64	13.98	0.988
		3	y = −4744.50x−4.48	39.45	13.40	0.987
		5	y = −4758.22x−4.4	39.56	13.83	0.987
	350–550	0	y = −11650.0x+ 2.42	96.86	259.5	0.979
		1	y = −11654.4x+ 2.43	96.89	257.3	0.979
		3	y = −11621.2x+ 2.38	96.62	268.9	0.979
		5	y = −11609.2x+ 2.36	96.52	273.7	0.979
	550–900	0	y = −8193.00x−5.59	68.12	7.679	0.962
		1	y = −8588.09x−5.17	71.40	12.21	0.966
		3	y = −9080.97x−4.69	75.50	20.86	0.964
		5	y = −9504.56x−4.28	79.02	32.77	0.963

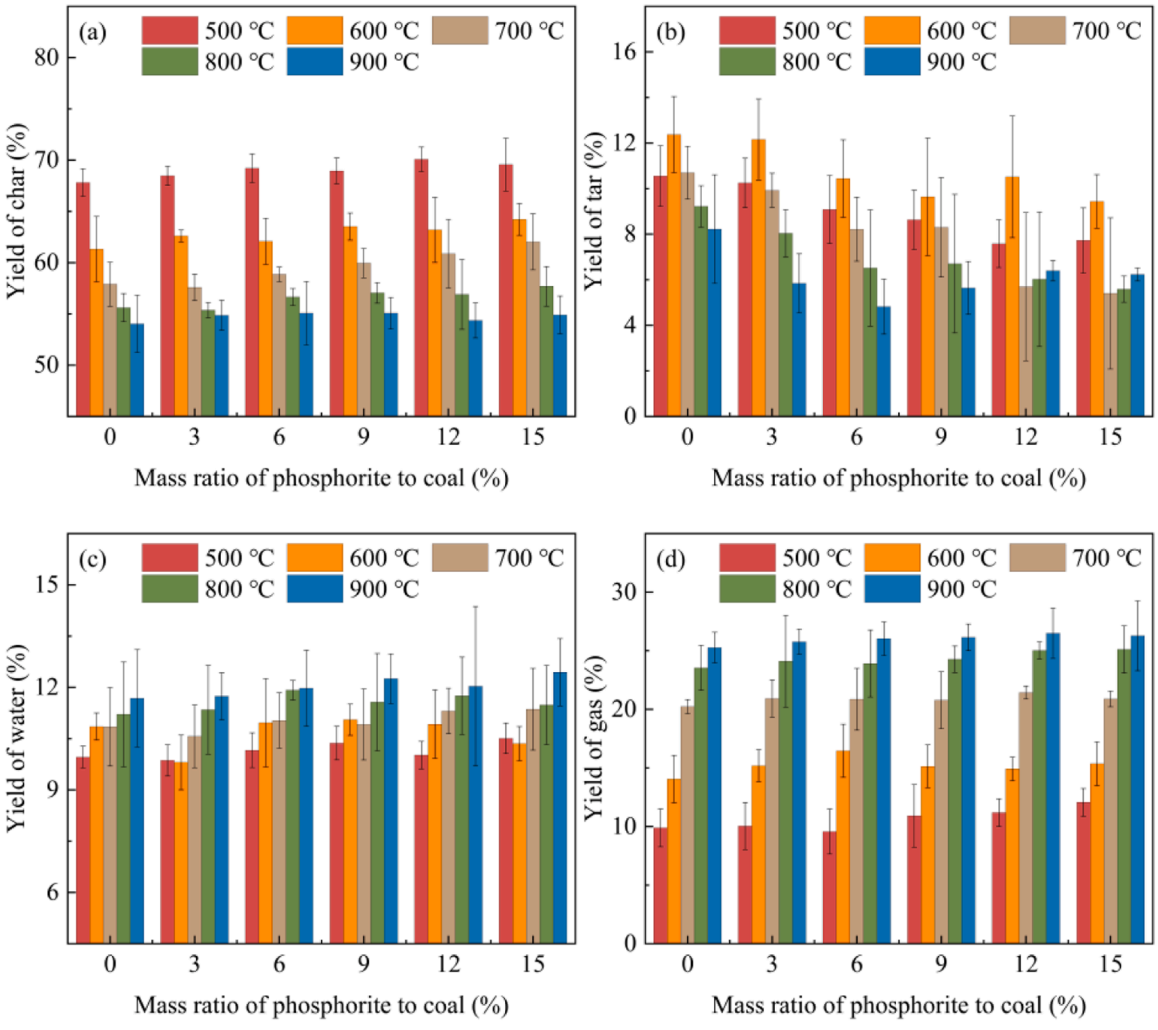

Fig. 3. Yield of pyrolysis products at different temperatures and mass ratios of phosphorite to NM coal.

without phosphorite.

3.2. The impact of co-pyrolysis on the pyrolysis products

This experiment conducted three parallel experiments for each condition, and the experimental results are summarized in Fig. 3 and Fig. 4. The mass loss of coal mainly comes from the decomposition of macromolecular organic matter or functional groups in coal, generating tar, pyrolysis water and pyrolysis gas, and the remaining solid product is char. The sum of the yields of the four products collected in each experiment is usually less than 100 %. This is because some experimental errors occur when collecting the products. Tar and water may be lost in small amounts in the transmission pipeline. The capture efficiency of pyrolysis gas may be insufficient. Meanwhile, the sensitivity and accuracy of the measurement system will also affect the final results. Therefore, this study performed a material balance calculation for the pyrolysis products. The total amount of products measured in the experiment deviated from the mass of the original coal sample by less than 2.5 %, which is still within the acceptable error range.

Fig. 3 and Fig. 4 illustrate that in the low temperature stage, the initial mass loss is small because the coal contains more moisture and volatiles. As the pyrolysis temperature increases, the release of volatiles in the gas phase and liquid phase increases, and the mass loss of the coal will increase. In the high temperature stage, the pyrolysis reaction is more intense and the mass loss increases significantly. Under an inert atmosphere, the yields of pyrolysis products (char, tar, pyrolysis water, and pyrolysis gas) for both NM coal and HM coal undergo significant changes as the pyrolysis temperature increases from 500 °C to 900 °C. As the temperature rises, the pyrolysis reactions intensify, releasing more volatile components, which increases the production of pyrolysis gas and tar while reducing char yield. Specifically, the char yield for NM coal decreases from 67.81 % to 54.03 %, and for HM coal, it decreases from 67.83 % to 51.32 %. Pyrolysis gas primarily originates from the direct decomposition of organic functional groups (or side chains) in coal, as well as from gas-phase radical polymerization of volatiles [57]. With rising temperatures, components of coal that are more difficult to decompose start undergoing cracking reactions, leading to increased formation of char and tar. Consequently, pyrolysis gas is released in greater quantities at higher temperatures. The yield of pyrolysis gas from NM coal increases from 9.89 % to 25.27 %, while for HM coal, it increases from 13.79 % to 31.37 %.

At lower temperatures, the yield of tar increases with rising pyrolysis temperature. However, at higher temperatures, the secondary reaction rates of tar also increase, leading to more intense condensation and cracking reactions. At a certain temperature, the rate of secondary tar reactions surpasses its generation rate, resulting in a peak tar yield. Beyond this temperature, the tar yield decreases. The maximum tar yields for NM coal and HM coal are observed at 600 °C, with 12.37 % and 12.77 %, respectively. Among the four pyrolysis products, pyrolysis water exhibits the smallest variation in yield with temperature. As the temperature increased, the yield of pyrolysis water increased from 9.96 % to 11.68 % for NM coal and from 7.64 % to 10.30 % for HM coal.

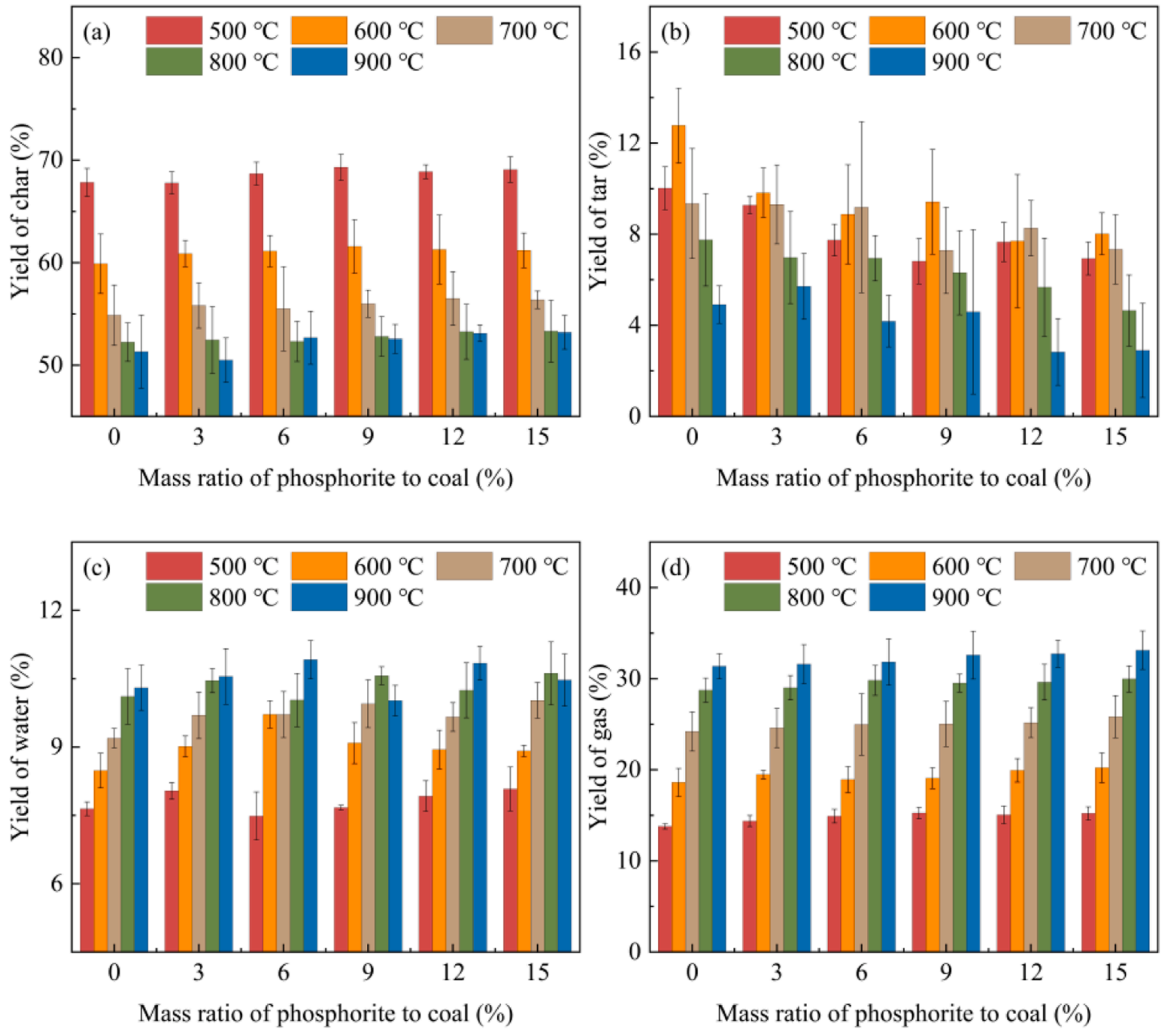

Fig. 4. Yield of pyrolysis products at different temperatures and mass ratios of phosphorite to HM coal.

Adding phosphorite significantly impacts the pyrolysis products of both NM coal and HM coal. Calcium fluoride phosphorite, rich in phosphorite, decomposes into CaO and $CaCO_3$ at high temperatures. Since these calcium-containing compounds promote the interaction between mineral components and organic matter in coal during the pyrolysis process and react with some functional groups to form macromolecular groups, this makes some carbon-based substances more difficult to volatilize, thereby reducing the mass loss rate of coal. CaO, with active sites on its surfaces, catalyzes tar condensation [58]. $CaCO_3$ bonds with oxygen-containing groups in coal, producing organic salt structures [59,60]. These interactions increase the pore volume and specific surface area of char, enhancing its activity [61,62], and facilitating tar condensation. Consequently, larger molecular groups remain in the char, and more small molecular gases are released.

Fig. 3 shows that as the amount of phosphorite increases, the yields of char and pyrolysis gas slightly increase, while the tar yield decreases significantly for both NM and HM coal. For NM coal, char yields increased by 1.76 %, 3.14 %, and 0.87 % at 500 °C, 700 °C, and 900 °C, respectively. Pyrolysis gas yields increased by 2.17 %, 0.65 %, and 1.01 %, respectively, while tar yields decreased by 2.83 %, 5.29 %, and 1.99 %, respectively. This indicates that the addition of phosphorite has a more significant effect at lower temperatures, with its influence diminishing as the temperature increases. Fig. 4 indicates a similar trend for HM coal.

The variation in pyrolysis water yield with phosphorite addition is minor, showing a slight overall increase. The increase is primarily due to CaO promoting the interaction of hydroxyl groups in coal, resulting in water removal. Additionally, phosphorite promotes polymerization reactions between molecular groups, generating CO_2 and H_2, with the reversible reaction ($CO + H_2O \leftrightharpoons CO_2 + H_2$) proceeding in the reverse direction, slightly increasing the pyrolysis water yield. After adding 15 % phosphorite by coal mass, the pyrolysis water yield of NM coal and HM coal increased by 0.51 % and 0.83 %, respectively, at 700 °C.

Fig. 5 and Fig. 6 illustrate the variations in four pyrolysis gas components (CO_2, CO, H_2, and CH_4) of NM coal and HM coal with different amounts of added phosphorite at various temperatures. During pyrolysis, CO_2 primarily originates from the decomposition of oxygen-containing functional groups in coal and carbonate minerals. When the pyrolysis temperature increased from 500 °C to 700 °C, the mass of CO_2 produced by NM coal increased by 310.51 $mg{\cdot}g^{-1}$. However, its relative content decreased by 6.80 %. At higher pyrolysis temperatures, the change in CO_2 mass generated by NM coal was minimal. Compared to a pyrolysis temperature of 700 °C, the relative content of CO_2 in the pyrolysis gas from NM coal decreased by 14.31 % at 900 °C. The mass of CO_2 generated by HM coal during pyrolysis is less affected by the pyrolysis temperature. When the pyrolysis temperature increased from 500 °C to 900 °C, the mass of CO_2 generated by HM coal increased by only 47.22 $mg{\cdot}g^{-1}$, while its relative content decreased by 35.39 %. As the pyrolysis temperature increases, the stable oxygen-containing functional groups in coal decompose to form CO [63,64]. With the increase in pyrolysis temperature, both NM coal and HM coal show an increasing trend in the mass of CO generated. Between 500 °C and 900 °C, NM coal and HM coal produced 646.01 $mg{\bullet}g^{-1}$ and 751.91 $mg{\bullet}g^{-1}$ of CO, respectively, with their relative contents increasing by 15.55 % and

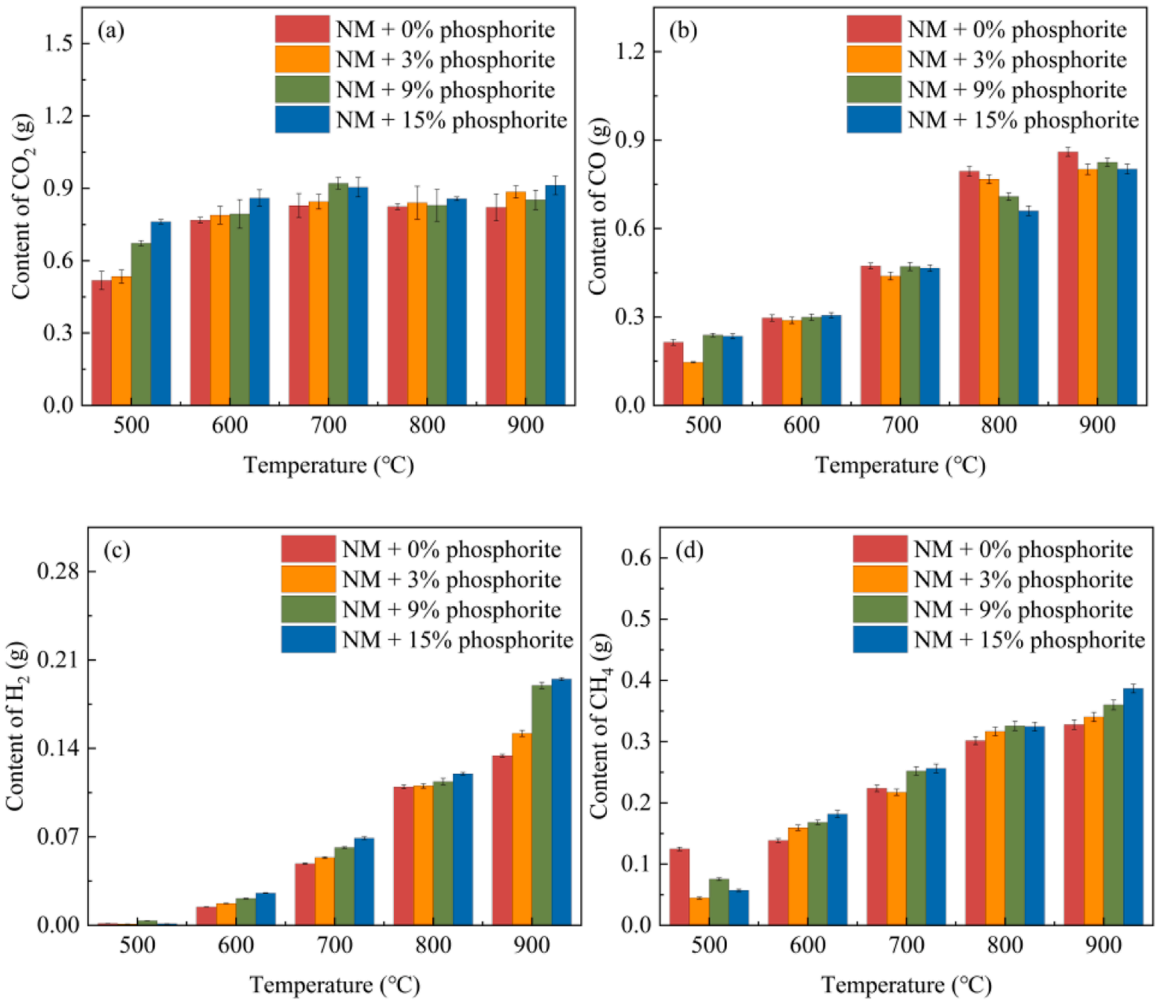

Fig. 5. Content of pyrolysis gas components at different temperatures and mass ratios of phosphorite to NM coal.

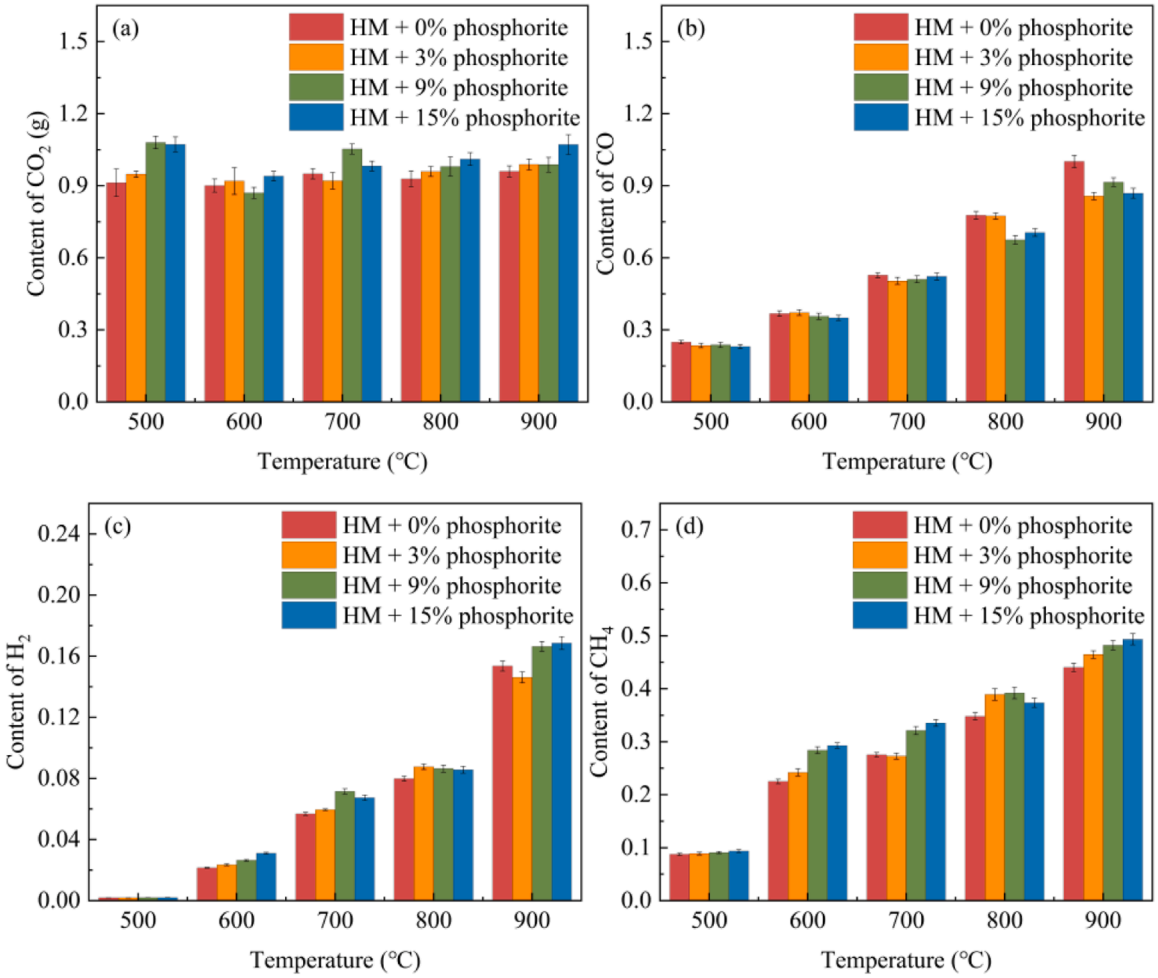

Fig. 6. Content of pyrolysis gas at different temperatures and mass ratios of phosphorite to HM coal.

19.28 %, respectively. Higher pyrolysis temperatures promote cracking and condensation reactions, leading to the generation of more H_2 and CH_4 [65]. When the coal is pyrolyzed at 500 °C, the generation of H_2 is almost negligible, indicating incomplete pyrolysis at this temperature. As the pyrolysis temperature increases, there is a significant increase in the generation of H_2. At 900 °C, 152.22 mg·g^{-1} and 153.53 mg·g^{-1} of H_2 are produced by NM coal and HM coal pyrolysis, respectively, with their relative contents being 6.26 % and 6.01 %, respectively. Both NM coal and HM coal show a significant increase in the mass of CH_4 generated during pyrolysis. When the pyrolysis temperature increases from 500 °C to 900 °C, the mass of CO produced by NM coal and HM coal pyrolysis increases by 202.97 mg•g^{-1} and 352.79 mg•g^{-1}, respectively.

Fig. 5 and Fig. 6 illustrate that the addition of phosphorite similarly affects the pyrolysis of both NM coal and HM coal. Irrespective of the pyrolysis temperature, adding phosphorite increases the generation of CO_2 and decreases the generation of CO. Calcium-based compounds can reduce the temperature at which gases such as H_2 and CH_4 are released [66]. At elevated temperatures, CaO derived from phosphorite not only promotes the dehydrogenation of methyl side chains from aromatic rings, forming char and H_2 [67], but also facilitates the dealkylation of aromatic components to form CH_4 [68]. Therefore, the addition of phosphorite increases the yields of H_2 and CH_4. CaO generated from phosphorite at high temperatures undergoes reactions as shown in (R3–8). According to existing research [69,70], during pyrolysis, the addition of alkali metals including calcium causes non-carboxyl oxygen-containing functional groups that would normally decompose into CO or remain in char and tar to react with the alkali metals, forming carbonates. Due to the small amount of added calcium-containing alkali metals, a small amount of CO undergoes the above reaction, resulting in a slight decrease in CO generated during pyrolysis. The formed carbonates spontaneously decompose at high temperatures, releasing CO_2 and thereby increasing the yield of CO_2.

3.3. The impact of co-pyrolysis on tar

This experiment utilized a Shimadzu GCMS QP2010 Plus gas chromatography-mass spectrometry (GC-MS) system to analyze small to medium-sized organic molecules in tar solutions. Quantitative analysis was conducted using area normalization. The injection volume of the tar sample was 1 μL, with a high-purity He atmosphere, a split flow rate of 6 mL/min, and a split ratio of 5:1. The temperature program was set as follows: an initial temperature of 50 °C held for 3 minutes, followed by a ramp at 10 °C/min to 300 °C, and held for 10 minutes. Fig. 7 presents the total ion chromatograms of tars produced from NM coal and HM coal under various conditions. Fig. 8 shows the relative proportions of different carbon chain lengths in the tar produced from NM coal and HM coal pyrolysis. Fig. 9 illustrates the relative proportions of fatty hydrocarbon (FH), fatty hydrocarbon derivative (FHD), monocyclic aromatic hydrocarbons (MAH), polycyclic aromatic hydrocarbons (PAH), and phenols (PH) in the tar produced from NM coal and HM coal pyrolysis. It is evident from these figures that both temperature variations and the addition of phosphorite influence the composition of tars generated during the pyrolysis of NM coal and HM coal.

At 500 °C, NM coal tar contains 28.52 % of components with carbon chain lengths shorter than C_{10}. This proportion increases to 43.12 % at 800 °C. As the pyrolysis temperature increases from 500 °C to 800 °C,

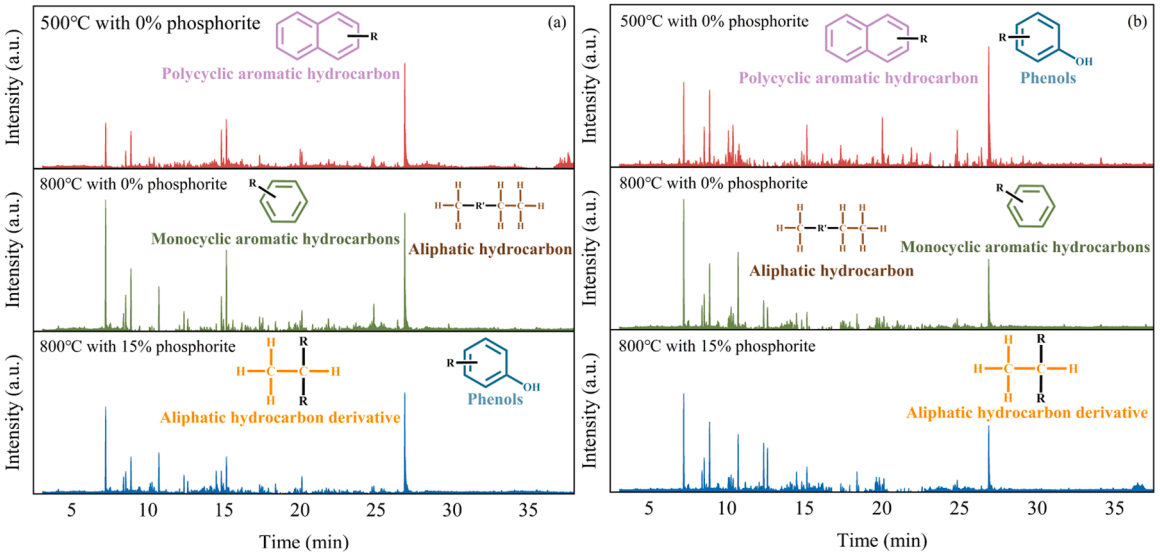

Fig. 7. TIC from GC-MS analysis of tars from the pyrolysis of NM coal (a) and HM coal (b).

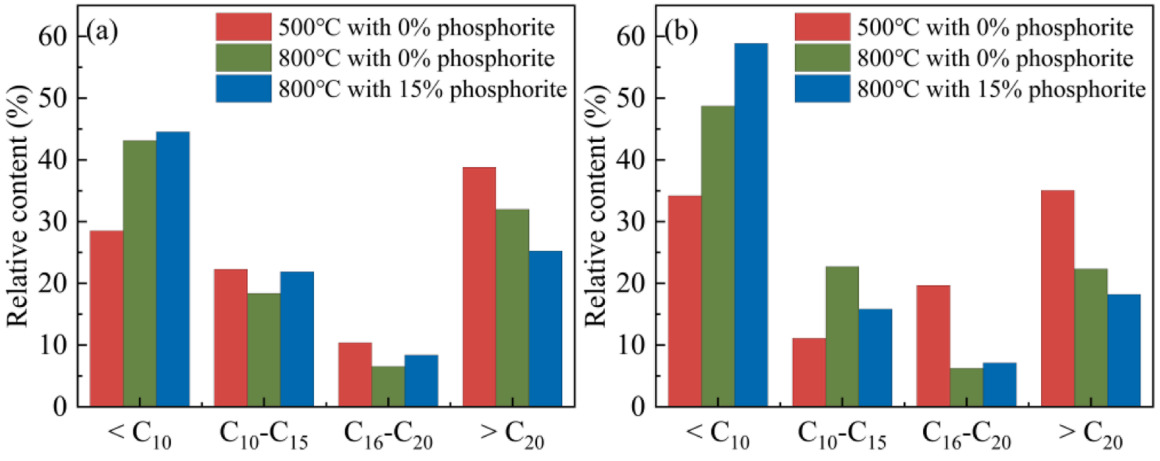

Fig. 8. Carbon chain length of NM coal (a) and HM coal (b) pyrolysis tars.

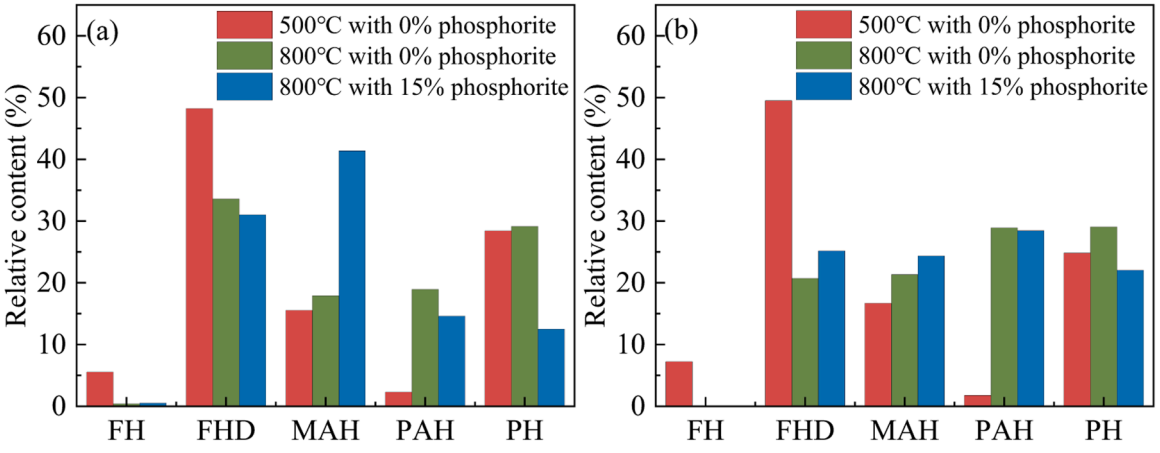

Fig. 9. Composition of NM coal (a) and HM coal (b) pyrolysis tars.

the proportions of components with carbon chain lengths of C_{15}-C_{20} and greater than C_{20} decrease by 3.86 % and 6.85 %, respectively. This indicates that higher pyrolysis temperatures intensify the pyrolysis reactions, promoting the decomposition of longer carbon chain components into shorter molecules, and increasing the proportion of shorter chain components. The proportion of longer chain components decreases significantly due to enhanced cracking and secondary cracking reactions at higher temperatures. HM coal tar exhibits a similar

trend during pyrolysis, where the proportions of components with carbon chain lengths C_{15}-C_{20} and longer than C_{20} decrease by 26.14 % from 500 °C to 800 °C. The addition of phosphorite results in a change in the composition of the tar derived from both the NH coal and HM coal. At 800 °C, NM coal tar shows a 4.91 % increase in components with carbon chain lengths shorter than C_{15}, while the proportion of components with carbon chain lengths longer than C_{20} decreases by 6.77 %. In HM coal tar, the proportion of components with carbon chain lengths shorter than C_{10} increases by 10.16 %, while those longer than C_{20} decrease by 4.15 %. This demonstrates that the introduction of calcium-containing compounds catalyzes cracking, facilitating the transformation of long-chain macromolecules in tar into shorter-chain molecules during pyrolysis. Generally, in industrial production, tar containing more short carbon chain components (especially carbon chains between C_5 and C_{15}) is considered to be a more ideal product. Short carbon chain components are smaller in size and exhibit weaker intermolecular forces, making them more chemically reactive and easier to convert into gaseous products. Their higher volatility and superior combustion characteristics contribute to lower emissions of harmful substances during coal combustion, thus mitigating environmental pollution. Therefore, adding phosphorite during pyrolysis can effectively improve the quality of tar.

Fig. 9 shows that varying the pyrolysis temperature significantly affects the composition of tar from both NM coal and HM coal. At higher temperatures, heteroatom-containing hydrocarbon derivatives become less stable and more prone to decomposition, and larger molecular weight fatty hydrocarbons are more susceptible to thermal cracking into smaller molecules [71]. Therefore, compared to pyrolysis at 500 °C, the proportion of fatty substances in tar decreases, while the proportion of aromatic substances increases at 800 °C. At 500 °C, NM coal tar consists of 53.76 % FH and FHD, with PAH accounting for 2.29 %. By 800 °C, the proportions of FH and FHD decrease by 19.76 %, while PAH increases by 16.64 %. The variation in HM coal tar composition with pyrolysis temperature is similar to NM coal. From 500 °C to 900 °C, FH and FHD decrease by 36.01 %, PAH increases by 27.12 %, and PH increases by 4.24 %. This indicates that higher pyrolysis temperatures favor the production of aromatic substances, especially polycyclic aromatic hydrocarbons. At the same pyrolysis temperature, adding 15 % phosphorite relative to coal mass reduces the proportion of fatty hydrocarbons and their derivatives in NM coal tar. The most significant change in tar composition is observed in aromatic compounds. The proportion of PH decreases from 29.16 % to 12.50 %, and PAH decreases from 18.94 % to 14.60 % with phosphorite addition. Meanwhile, the proportion of MAH increases significantly when phosphorite is present, showing a 23.47 % increase compared to pyrolysis without phosphorite. This indicates that calcium-containing compounds catalyze the cracking of polycyclic aromatic hydrocarbons into monocyclic aromatic hydrocarbons or other smaller molecular compounds, thereby altering the tar composition. These findings are consistent with studies by Zhu et al. [72] and Chang [73] regarding changes in tar composition with the addition of CaO during coal pyrolysis. Phosphorite-assisted pyrolysis also affects HM coal tar composition. After adding phosphorite, the proportion of MAH in HM coal tar increases by 3.04 %, while PH decreases by 7.01 %. Despite these changes being relatively minor, the pattern aligns with that observed in NM coal, confirming that calcium-containing compounds catalyze the cracking of aromatic compounds and reactions of phenolic substances during pyrolysis. During the pyrolysis process, PAH and PH in tar are difficult to burn completely due to their high molecular structure, and the combustion residues are easy to accumulate in the environment, causing persistent pollution. In addition, these compounds are corrosive and toxic. The addition of phosphorite promotes their cracking, generating MAH and small molecular substances with higher reactivity and easy to further decompose. These components are highly volatile and degrade quickly, reducing pollution to the environment. Therefore, co-pyrolysis of phosphorite and low-rank coal helps to lighten tar, improve its ability to be separated into high-quality chemicals, and reduce the emission of impurities and heavy components during combustion, reducing toxicity and pollution.

3.4. The impact of co-pyrolysis on the functional groups of char

Fig. 10 presents the FTIR spectra of NM coal and HM coal co-pyrolyzed with varying amounts of phosphorite at 700 °C. According to the Beer-Lambert law, the intensity or area of absorption peaks in the infrared spectra is directly proportional to the concentration of components in the sample [74,75]. Li et al. [76] provided detailed descriptions of the peak assignments in the FTIR spectra. In the spectra, the region from 3600 to 3000 cm^{-1} primarily corresponds to the stretching vibration peaks of hydroxyl groups (OH). The range from 1800 to 1300 cm^{-1} exhibits absorption peaks of oxygen-containing functional groups such as carboxyl (COOH) and carbonyl (C═O). The region from 1300 to 1000 cm^{-1} shows absorption peaks of ethers (alkyl ether C-O-C and aromatic ether R-C). The range from 900 to 700 cm^{-1} mainly represents the absorption peaks of aromatic hydrocarbon C-H bonds.

Fig. 10 illustrates that the infrared spectra of the pyrolyzed char from NM coal and HM coal exhibit pronounced peaks in the 3600–3000 cm^{-1} region. This is attributed to the strong bond energy of the -OH group, which undergoes minimal functional group cleavage during moderate to low-temperature pyrolysis [77]. Upon the addition of phosphorite, a notable decrease in the intensity of the -OH peaks is observed in both coal samples. This phenomenon occurs as a result of the calcium-based compounds in the phosphorite reducing the bond energy of the -OH group, which in turn facilitates the cleavage of these functional groups. Additionally, CaO released from the reaction of $Ca_5(PO_4)_3$ with SiO_2 can react with -OH, further reducing the content of the -OH group.

$$\text{R-C-OH} + \text{CaO} + \text{R'-C-OH} \rightarrow \text{R-C-O-Ca-O-C-R'} + H_2O \quad \text{(R9)}$$

$$\text{R-COOH} + \text{CaO} + \text{R'-COOH} \rightarrow \text{R-COO-Ca-COO-R'} + H_2O \quad \text{(R10)}$$

$$\text{R-C-O-Ca-O-C-R'} + CO_2 \rightarrow \text{R-C-O-C-R'} + CaCO_3 \quad \text{(R11)}$$

$$\text{R-COO-Ca-COO-R'} \rightarrow \text{R-C-O-C-R'} + CaCO_3 \quad \text{(R12)}$$

The infrared spectra of the pyrolyzed char demonstrate that the characteristic peaks of both coals in the 1800–1300 cm^{-1} region gradually decrease in intensity with increasing phosphorite addition. This indicates that the addition of phosphorite facilitates the cleavage reaction of -COOH functional groups during coal pyrolysis, resulting in a lower content of -COOH functional groups in the char. In the absence of phosphorite addition, the characteristic peaks in the 1300–1000 cm^{-1} region are weaker in the char derived from both coals. However, following the addition of phosphorite, these peaks demonstrate an increase in intensity, indicative of an elevated content of the C-O-C functional group. CaO reacts with carboxyl and hydroxyl groups to undergo dehydration, forming unstable structures such as O-Ca-O and COO-Ca-COO at high temperatures. These structures readily decompose into ether groups (C-O-C) when subjected to further thermal processing. Therefore, during pyrolysis with phosphorite addition, the content of hydroxyl (-OH), carboxyl (-COOH), and analogous functional groups in the char decreases, while the content of ether groups C-O-C increases. This phenomenon also explains why the addition of phosphorite to coal enhances the yield of water during pyrolysis, corroborating the preceding analysis.

In conclusion, CaO produced from the decomposition of phosphorite at high temperatures reacts with the coal in a manner consistent with the proposed reactions (R9–12). The characteristic peaks of the char from co-pyrolysis of phosphorite with coal in the 900–700 cm^{-1} region exhibit a slight elevation in comparison to those of char directly derived from the coal. This elevation is observed to increase with an increase in phosphorite addition. As this region is primarily associated with the stretching vibrations of aromatic hydrocarbon C-H bonds, this indicates that phosphorite inhibits the cleavage of aromatic hydrocarbon C-H bonds during pyrolysis, consequently reducing the formation of liquid

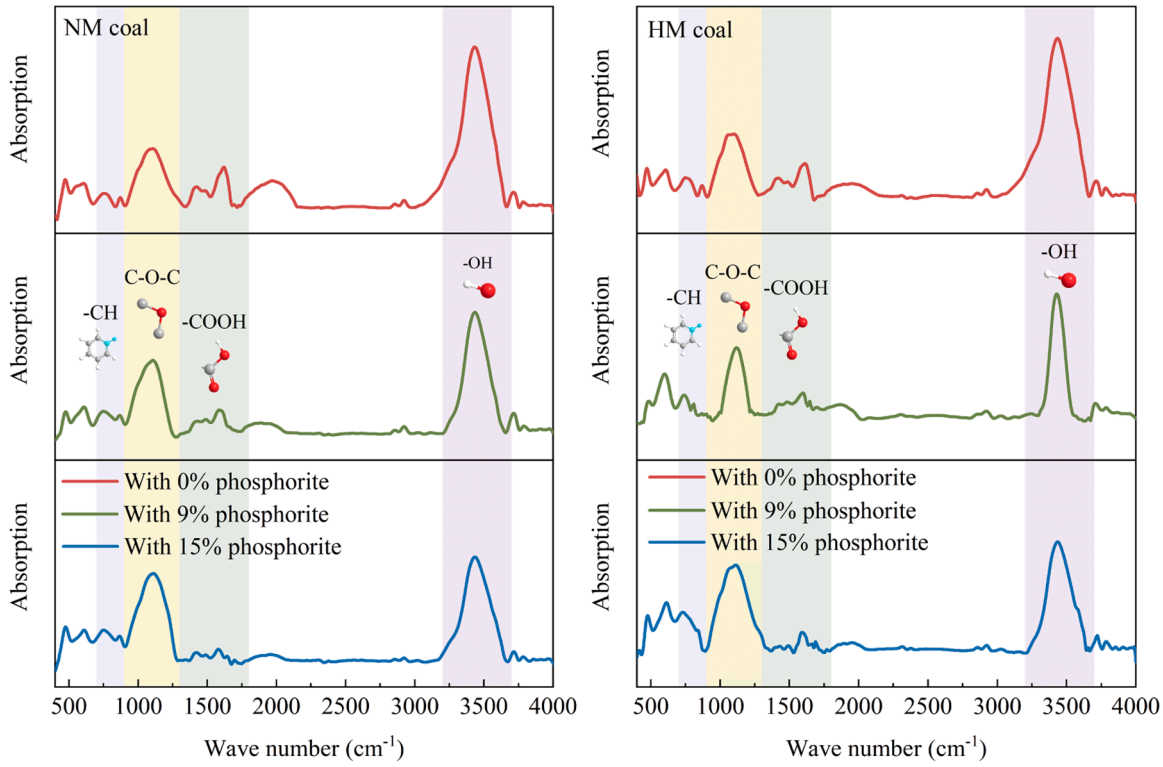

Fig. 10. FTIR spectra of pyrolysis char under various experimental conditions (a)NM coal, (b) HM coal.

small molecule aromatic hydrocarbons. This finding aligns with the previous analysis of pyrolysis kinetics and explains the increased char yield and reduced tar yield observed after the addition of phosphorite.

3.5. The impact of co-pyrolysis on the migration of Na and Cl

Two distinct coal samples, NM coal and HM coal, were individually taken at a mass of 0.1 g and subsequently subjected to digestion. The resulting solutions were diluted to 100 mL with deionized water, and the sodium (Na) content in the solutions was determined using an ion chromatograph. According to the ASTM E1915–97 standard, which employs the pyridine-pyrazolone titration method, the chlorine (Cl) content in the two coals was measured. The sodium (Na) contents in NM coal and HM coal were 0.51 % and 0.34 %, respectively, while their chlorine (Cl) content was 0.39 % and 0.43 %, respectively. Referring to standards MT/T 1074–2007 and GB/T 20475.2–2006, NM coal is classified as high-sodium, high-chlorine coal, while HM coal is categorized as medium-sodium, high-chlorine coal.

During pyrolysis, substantial quantities of Na and Cl elements are released into the pyrolysis gas. These elements have the potential to deposit on the surface of pipelines and corrode exposed heating surfaces when combined with acidic gases, thereby severely affecting boiler operation. Due to challenges in directly measuring Na and Cl concentrations in gases and the uncertainty regarding their forms in both the gaseous and solid phases, a simulation was conducted with Factsage software to study the migration of Na and Cl elements during coal pyrolysis. The simulations analyzed the release rates and chemical forms of Na and Cl from the two coals under different temperatures and varying amounts of phosphorite addition, to infer potential chemical reactions and establish a theoretical foundation for industrial applications.

A series of calculations were conducted using Factsage software to model the pyrolysis process of Shaer Lake coal under a nitrogen atmosphere, employing the equilibrium model. A mass of 1000 g of coal ash was subjected to simulated pyrolysis at temperatures ranging from 400 °C to 1000 °C, with increments of 100 °C, in an atmosphere of excess nitrogen gas. Table 1 shows the ash composition of two low-rank coals and phosphorite, and Table 2 shows the industrial analysis results of two low-rank coals. Based on the data shown in Table 1 and Table 2, 14 initial elements and their contents can be calculated: C, H, N, O, S, Si, Al, Fe, Ca, Mg, S, K, Na and Cl. The results are presented in Table 4.

Following the calculations, the phase compositions of Na and Cl produced during the pyrolysis of NM coal and HM coal at different temperatures and various phosphorite addition ratios were determined. The results are presented in Fig. 11.

Fig. 11 illustrates the release and migration of Na and Cl during the pyrolysis of NM coal, as the results of the experiment and simulation. Thermodynamic calculations indicate that Na in NM coal begins to release into the gas phase at pyrolysis temperatures exceeding 700 °C. The proportion of gas-phase Na compounds increases rapidly with rising pyrolysis temperature, reaching 33.31 % at 1000 °C. The addition of phosphorite during pyrolysis has been observed to significantly reduce the proportion of gas-phase Na compounds. When the proportion of phosphorite added to the coal mass exceeds 10 %, only a small quantity of Na enters the gas phase at temperatures exceeding 900 °C. The addition of phosphorite to NM coal at a ratio of 15 % by mass, followed by pyrolysis at 1000 °C, results in a gas-phase Na compound proportion of only 1.43 %.

At pyrolysis temperatures below 700 °C, solid-phase Na compounds primarily exist as NaCl (s) and $Na_2Ca_3Si_6O_{16}$ (s). At temperatures exceeding 800 °C, some NaCl (s) undergoes a gradual conversion to NaCl (g) or $(NaCl)_2$ (g), releasing into the gas phase. Meanwhile, the remaining NaCl (s) reacts with Al_2O_3 and SiO_2 to form $NaAlSiO_4$ residue in the solid phase. As the temperature rises, $Na_2Ca_3Si_6O_{16}$ (s) undergoes a reaction with Al_2O_3, resulting in the formation of $NaAlSiO_4$ (s) and $CaAl_2SiO_8$ (s). The addition of phosphorite introduces a significant quantity of Al_2O_3 and SiO_2, resulting in the formation of a considerable amount of $NaAlSi_3O_8$ (s) in the pyrolysis products. At temperatures exceeding 900 °C, $NaAlSi_3O_8$ (s) undergoes thermal decomposition, releasing in the release of NaCl (g) and a minor quantity of $(NaCl)_2$ (g). This process enables the retention of a greater proportion of Na within

Table 4
Mole composition data of pyrolysis material.

Sample/mol	C	H	O	N	S	Cl	Si	Al	Fe	Ca	Mg	Na	K	P
NM coal	60.6	3.78	16.3	0.95	0.24	0.39	2.68	0.64	0.51	1.78	0.29	0.46	0.03	0.00
NM coal+ 3 %PH	60.6	3.78	16.3	0.95	0.24	0.39	3.77	0.87	0.54	2.48	0.45	0.47	0.06	0.65
NM coal+ 5 %PH	60.6	3.78	16.3	0.95	0.24	0.39	6.32	1.41	0.63	4.09	0.82	0.48	0.12	2.15
NM coal+ 10 %PH	60.6	3.78	16.3	0.95	0.24	0.39	8.14	1.79	0.69	5.25	1.08	0.49	0.16	3.23
HM coal	67.9	4.46	14.9	1.06	0.3	0.43	2.20	1.49	1.46	3.51	0.42	0.35	0.03	0.00
HM coal+ 3 %PH	67.9	4.46	14.9	1.06	0.3	0.43	3.29	1.73	1.49	4.21	0.58	0.36	0.05	0.65
HM coal+ 5 %PH	67.9	4.46	14.9	1.06	0.3	0.43	5.84	2.26	1.58	5.82	0.95	0.37	0.11	2.15
HM coal+ 10 %PH	67.9	4.46	14.9	1.06	0.3	0.43	7.66	2.65	1.64	6.98	1.21	0.38	0.16	3.23

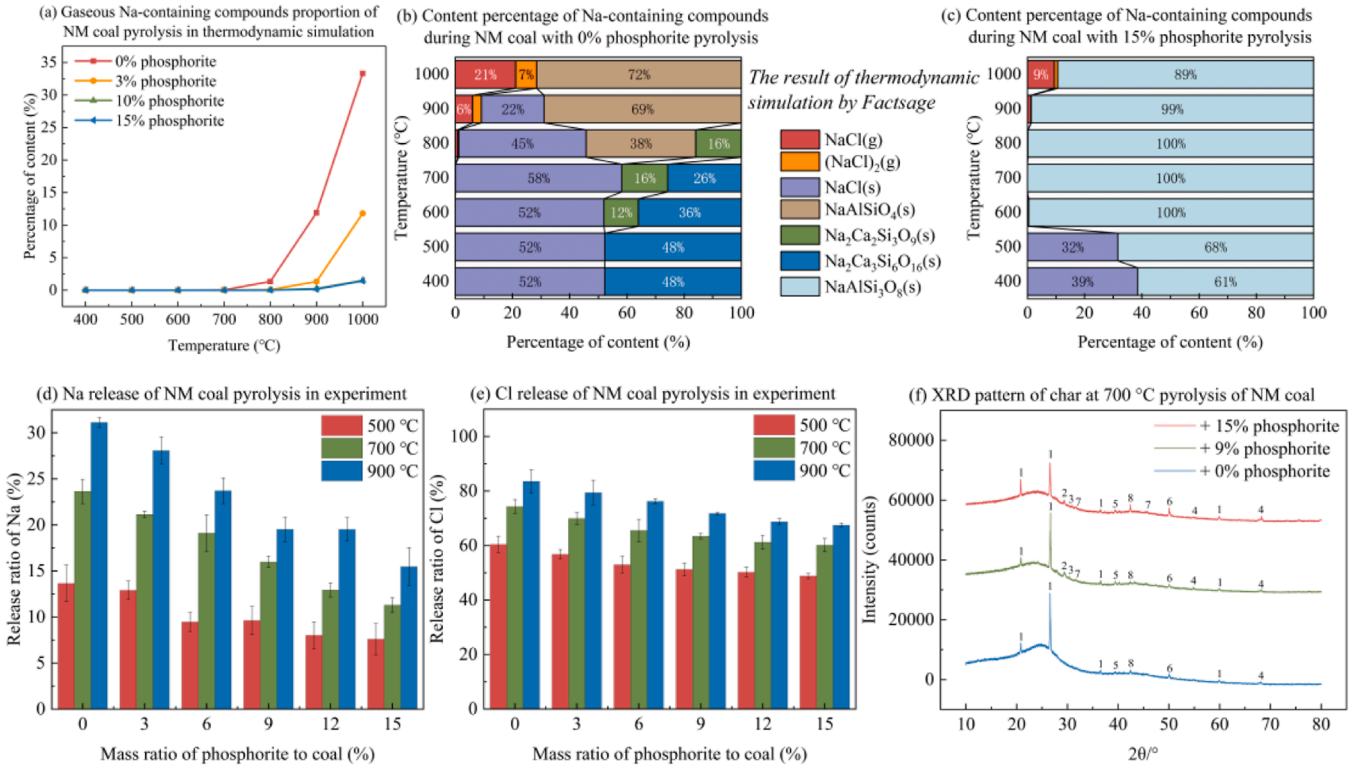

Fig. 11. Simulation and experimental results of migration and release of Na and Cl during the pyrolysis of NM coal.

the solid phase.

The results calculated by Factsage software indicate that chloride compounds are primarily present as NaCl (s) and KCl (s) at lower pyrolysis temperatures. The addition of phosphorite results in an increase in HCl production at higher pyrolysis temperatures. The resulting HCl then reacts with oxygen-containing compounds such as CaO, $Ca_3(PO_4)_2$, MgO, and Fe_2O_3 present in the coal and phosphorite. The resulting products are stable, occurring in solid-phase and including $CaCl_2$, $MgCl_2$, and $FeCl_3$. Therefore, the gas-phase content of chlorine is diminished following the addition of phosphorite. The reduction in gas-phase Na and Cl compounds is beneficial for mitigating deposition and corrosion issues on heat-exposed boiler surfaces, thereby enhancing the operational safety of the equipment.

$$6NaCl + 4Ca_5(PO_4)_3F + SiO_2 \rightarrow 3CaCl_2 + SiF_4 + 2Na_3PO_4 + 5Ca_3(PO_4)_2 + 2CaO \quad (R13)$$

$$3SiF_4 + 2Al_2O_3 + 6NaCl \rightarrow 2Na_3AlF_6 + 3SiO_2 + 2AlCl_3 \quad (R14)$$

$$4NaCl + 6CaO + 13SiO_2 \rightarrow 2Na_2Ca_3Si_6O_{16} + SiCl_4 \quad (R15)$$

$$SiCl_4 + H_2O \rightarrow HCl + H_2SiO_3 \quad (R16)$$

$$H_2SiO_3 + CaO \rightarrow CaSiO_3 + H_2O \quad (R17)$$

$$6NaCl + 18SiO_2 + 4Al_2O_3 \rightarrow 6NaAlSi_3O_8 + 2AlCl_3 \quad (R18)$$

$$MgO + 3NaCl + 2CO_2 + H_2O \rightarrow Na_3Mg(CO_3)_2Cl + 2HCl \quad (R19)$$

$$HCl + CaO \rightarrow CaCl_2 + H_2O \quad (R20)$$

As illustrated in Fig. 11, the observed trends in Na and Cl release demonstrate a gradual decrease with increasing phosphorite addition. At a temperature of 500 °C, pyrolysis of NM coal results in the release of 13.65 % Na and 60.43 % Cl into the gas phase. The addition of phosphorite has a significant impact on the amounts of Na and Cl released during NM coal pyrolysis, with greater phosphate addition resulting in a notable decrease in these quantities. The addition of 15 % phosphorite relative to the mass of the coal results in the release of 7.60 % Na and 48.80 % Cl into the gas phase during the pyrolysis of NM coal.

The impact of phosphorite on the reduction of sodium and chloride

release during pyrolysis is more pronounced at higher temperatures. At 900 °C, the addition of 15 % phosphorite relative to the mass of the coal results in a reduction of the release of Na and Cl by 15.67 % and 16.05 %, respectively, in comparison to the pyrolysis of NM coal without phosphorite. Referring to the previous research methods [39,78,79], XRD analysis and data processing were carried out on the char produced under different conditions. As evidenced by the XRD spectra of the char produced from pyrolysis at 700 °C, the addition of phosphorite results in a notable decrease in the intensity of the characteristic peak of SiO_2, while the intensities of the characteristic peaks of $Na_2Ca_3Si_6O_{16}$ and $Na_3Mg(CO_3)_2Cl$ exhibit a slight increase. Furthermore, new characteristic peaks of $CaCl_2$ and $NaAlSi_3O_8$ appear in the characteristic peaks of the char. This indicates that the NaCl and SiO_2 present in the coal react with the $Ca_5(PO_4)_3F$ introduced by the phosphorite to form $Na_2Ca_3Si_6O_{16}$. Additionally, some of the NaCl and SiO_2 react with the MgO and Al_2O_3 carried by the phosphorite to produce $Na_3Mg(CO_3)_2Cl$ and $NaAlSi_3O_8$. The reactions observed in these processes are depicted in (R13–20).

These findings corroborate the conclusions derived from thermodynamic calculations. The addition of phosphorite expedites reactions between Na- and Cl-containing compounds in coal and calcium-based compounds and alumina present in phosphorite, resulting in the formation of compounds with elevated melting points that are less volatile in the gas phase. This effectively reduces the content of Na and Cl in the pyrolysis gas, alleviating issues such as fouling, slagging, and corrosion on heat exchanger surfaces during pyrolysis.

Fig. 12 illustrates the release and migration of Na and Cl during the pyrolysis of HM coal. As illustrated in Fig. 12, the trends observed in simulations and experiments for HM coal are consistent with those observed for NM coal. The addition of phosphorite reduces the release of Na and Cl during the pyrolysis of HM coal. The experimental results demonstrate that at 900 °C, the addition of 15 % phosphorite relative to the coal mass results in a decrease in the release of Na and Cl by 11.17 % and 17.66 %, respectively, in comparison to the pyrolysis of HM coal without phosphorite.

As illustrated in Fig. 11 and Fig. 12, the experimental result indicates a higher release of Na than that predicted by the calculations. This discrepancy may be attributed to the simplification of chemical reactions in the simulation calculations, which may have overlooked certain secondary reactions or intermediate products that occur in reality. The coal may contain catalysts or promoters (such as certain metal oxides) that facilitate the release of Na. Volatiles (including sodium compounds) may undergo secondary reactions and rearrangements, resulting in the production of more volatile sodium compounds. These secondary reactions and rearrangements may not be accurately simulated in the calculations. Additionally, temperature gradients and distributions within the reactor during actual experiments could result in the formation of localized high-temperature zones. Fluctuations in temperature and pressure may also contribute to the dynamic promotion of sodium release. These factors collectively may result in a higher measured Na release in experiments compared to the results of the thermodynamic calculation.

3.6. The impact of co-pyrolysis on phosphorite reduction

The prepared phosphorite was placed into a fixed-bed reactor. The reaction temperatures were set at 1150 °C, 1200 °C, and 1250 °C, with 5 min, 10 min, 15 min, 20 min, 30 min, 40 min, 60 min, and 80 min, respectively. Fig. 13 illustrates the conversion ratios of phosphorite directly participating in reduction reactions and phosphorite participating in reduction reactions during co-pyrolysis at different reaction times. The experimental data for phosphorite conversion ratios obtained

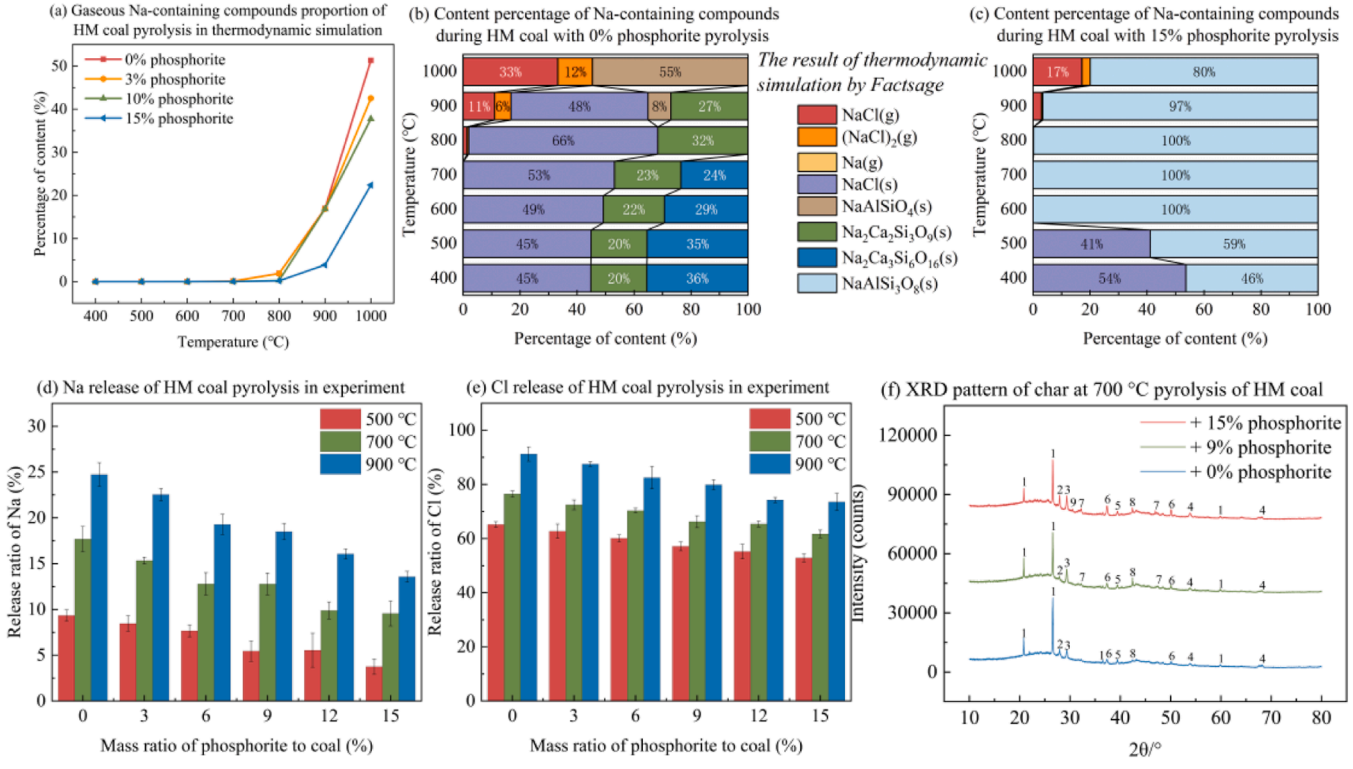

Fig. 12. Simulation and experimental results of migration and release of Na and Cl during the pyrolysis of HM coal.

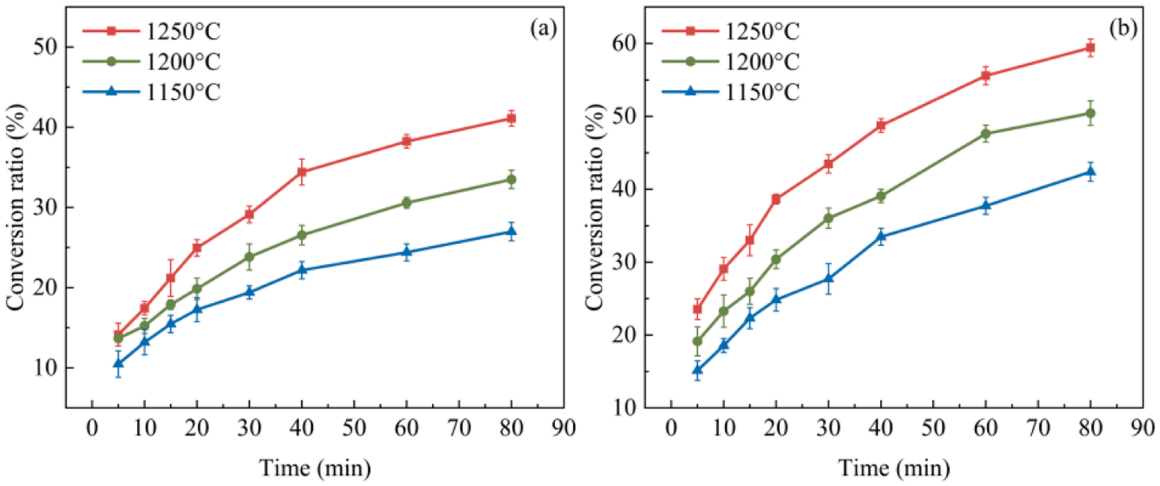

Fig. 13. Conversion ratio of phosphorite by carbothermal reaction: (a) Reduction of phosphorite, (b) Reduction of phosphorite co-pyrolyzed with coal.

from Fig. 13 were processed and fitted with curves.

As illustrated in Fig. 13, temperature has a pronounced effect on the conversion ratio of phosphorite. When phosphorite is directly involved in reduction reactions at 1150 °C, the conversion ratio of phosphorite reacting with carbon for 80 min is only 26.99 %. In contrast, at 1250 °C, the conversion ratio increases to 41.11 %. As the reaction time increases, regardless of whether co-pyrolysis with coal occurs, the conversion ratio of phosphorite continues to rise. During the initial stages of the reduction reaction, the temperature of the raw materials rises rapidly, resulting in a significant increase in the rate of phase change within the reaction system. This leads to the escape of a considerable amount of gaseous products, accelerating the heat and mass transfer processes and maximizing the driving force of the reaction, thereby achieving higher reaction rates.

After 40 min, the curve of phosphorite conversion ratio versus time gradually flattens, indicating a slowdown in the rate of increase due to significant consumption of raw materials. Specifically, when phosphorite is directly involved in reduction reactions, the conversion ratios at 20 min and temperatures of 1150 °C, 1200 °C, and 1250 °C are 17.26 %, 19.63 %, and 24.96 %, respectively. Extending the reaction time to 40 minutes resulted in an increase of these conversion ratios by 4.92 %, 6.91 %, and 9.45 %, respectively. Further extending the reaction time to 60 min results in increases of 2.22 %, 4.03 %, and 3.82 %, respectively, in comparison to the 40 min.

Fig. 13 **(b)** illustrates that the conversion ratio of phosphorite co-pyrolyzed with coal for carbon thermal reduction reactions exhibits a comparable trend concerning temperature and time is similar. In comparison to the direct reduction of phosphorite, the co-pyrolyzed phosphorite exhibits a higher conversion ratio under the same operating conditions. At temperatures of 1150 °C, 1200 °C, and 1250 °C, and a reaction time of 80 min, the conversion ratios of co-pyrolyzed phosphorite are 42.39 %, 50.43 %, and 59.41 %, respectively, representing increases of 15.40 %, 16.94 %, and 18.30 % over directly reduced phosphorite.

$$2Ca_5(PO_4)_3F + 15\,C \rightarrow 9CaO + CaF_2 + 15CO(g) + 3\,P_2(g) \quad (R21)$$

$$2Ca_5(PO_4)_3F + 9SiO_2 + 15\,C = 9CaSiO_3 + 3\,P_2\uparrow + 15CO\uparrow + CaF_2 \quad (R22)$$

$$6NaCl + 2Ca_5(PO_4)_3F \rightarrow 3CaCl_2 + CaF_2 + 2Na_3PO_4 + 2Ca_3(PO4)_2 \quad (R23)$$

$$6KCl + 2Ca_5(PO_4)_3F \rightarrow 3CaCl_2 + CaF_2 + 2K_3PO_4 + 2Ca_3(PO4)_2 \quad (R24)$$

$$3MgO + 2Ca_5(PO_4)_3F \rightarrow Mg_3(PO_4)_2 + CaF_2 + 2Ca_3(PO_4)_2 + 3CaO \quad (R25)$$

$$2Ca_5(PO_4)_3F + Al_2O_3 = 2AlPO_4 + CaF_2 + 2Ca_3(PO_4)_2 + 3CaO \quad (R26)$$

$$Ca_3(PO_4)_2 + 5\,C \rightarrow 3CaO + P_2(g) + 5\,CO(g) \quad (R27)$$

$$2Na_3PO_4 + 5\,C + 3SiO_2 \rightarrow 3Na_2SiO_3 + P_2(g) + 5\,CO(g) \quad (R28)$$

$$2K_3PO_4 + 5C + 3SiO_2 \rightarrow 3K_2SiO_3 + P_2(g) + 5CO(g) \quad (R29)$$

$$Mg_3(PO_4)_2 + 5C + 3SiO_2 \rightarrow 3MgSiO_3 + P_2(g) + 5CO(g) \quad (R30)$$

$$6AlPO_4 + 15\,C + 3SiO_2 \rightarrow 3Al_2SiO_5 + 3\,P_2(g) + 15CO(g) \quad (R31)$$

The reactions occurring during the carbon thermal reduction process of phosphorite are primarily concerned with the reaction of calcium fluorophosphate with carbon, resulting in the production of CO (g) and P_2 (g). This is illustrated in (R21–27). Prior research has demonstrated that the incorporation of alkali metal compounds containing Mg and Al can effectively reduce the initial reaction temperature and enhance the conversion ratio of the reduction reaction [80,81]. The addition of compounds containing K and Na to phosphorite has been observed to reduce the viscosity of the slag and lower the melting point of the reaction, thereby facilitating the transfer of substances between reactants and significantly enhancing the conversion ratio of phosphorite [82,83]. The NM coal and HM coal selected for this experiment contain substantial quantities of compounds with Mg, Al, K, Na, and other elements. These compounds react with components in the phosphorite during co-pyrolysis, not only forming various silicates that strengthen the molten state reduction process. Additionally, residual compounds such as $Ca_3(PO_4)_2$, Na_3PO_4, K_3PO_4, $AlPO_4$, $Mg_3(PO_4)_2$, and others are produced. According to Mckee et al. [84] and Shen et al. [85], in comparison to $Ca_5(PO_4)_3F$, $Ca_3(PO_4)_2$, Na_3PO_4, K_3PO_4, $Mg_3(PO_4)_2$, and $AlPO_4$ exhibit lower initial temperatures for reaction with carbon and are more readily reduced by carbon, thereby achieving higher conversion ratios. The reactions involved in these processes are illustrated in reactions (R28–31).

A kinetic analysis of the phosphorite reduction reaction in this study is presented in the supporting information. The results show that the activation energy of direct reduction of phosphorite is 119.85 kJ•mol^{-1}, and the activation energy of co-pyrolysis phosphorite reduction is 91.885 kJ•mol^{-1}. Compared with the reduction of untreated phosphorite, the activation energy of co-pyrolyzed phosphorite reduction is reduced by 27.965 kJ•mol^{-1}, indicating that co-pyrolyzed phosphorite with coal can significantly reduce the activation energy of the reaction system, increase the conversion ratio, and promote the reaction, thereby improving the utilization rate of phosphorite and reducing costs.

3.7. Innovation and significance

Table 5 shows previous studies on the addition of calcium-containing additives during coal pyrolysis. In previous studies, a large number of

Table 5
Summary of studies on the addition of calcium-containing additives to coal pyrolysis.

Year	Researchers	Additives	Addition Method	Research Findings
1991	Khan and Seshadri [86]	CaO and Genstar	Mechanical Mixing	CaO induces a variety of reactions during the pyrolysis of low-rank coal, including cracking and aromatization of alkanes.
2000	Zhu et al. [9]	CaO	Mechanical Mixing	The relative content of short-chain aliphatic hydrocarbons in tar increases, while the relative content of long-chain aliphatic hydrocarbons decreases.
2003	Tsubouchi et al. [87]	CaO	Mechanical Mixing	CaO promotes the formation of disordered graphite in char.
2004	Jia et al. [88]	CaO	Mechanical Mixing	Calcium compounds promote the polycondensation reaction of tar, reduce the yield of tar, and increase the calorific value of pyrolysis gas.
2007	Zou et al. [89]	$CaCl_2$	Impregnation	During the pyrolysis process, calcium will repeatedly form and break bonds with oxygen-containing functional groups in coal, decomposing the fatty components or small molecular aromatics in tar into gas and converting large molecular aromatics into char.
2011	Liu et al. [90]	$Ca(OH)_2$ and $CaCO_3$	Mechanical Mixing	During rapid pyrolysis, calcium-based compounds reduce the yield of tar and increase the yield of char.
2013	Liu et al. [91]	$Ca(OH)_2$, $Ca(CH_3COO)_2$, and $CaCO_3$	Mechanical Mixing	Regardless of the calcium compound and the method of addition, the CH4 yield from coal pyrolysis increases.
2013	Zhang et al. [61]	$Ca(OH)_2$	Impregnation	During low-rank coal gasification, a higher Ca content is more likely to cause catalyst particle coarsening and increase the char yield.
2022	Ban et al. [92]	$Ca(OH)_2$	Impregnation	Calcium improves the thermal conversion pathways of oxygen-containing functional groups in different aromatic structures, changes the composition of primary pyrolysis products, and promotes condensation between structures.
2023	Ban et al. [26]	Industrial waste carbide slag	Mechanical Mixing	Co-pyrolysis of industrial waste carbide slag and low-rank coal can reduce the content of benzene and phenolic compounds in tar and obtain high-quality tar.
2024	Wu et al. [30]	$CaCl_2$	Mechanical Mixing	$CaCl_2$ can reduce the release of tiny particles during the pyrolysis of low-rank coal and reduce the pollutant content in the flue gas.

scholars paid attention to the impact of calcium-based additives on the coal pyrolysis process. Represented by calcium-based compounds such as CaO, $Ca(OH)_2$, $CaCO_3$, and $CaCl_2$, these additives are added to the pyrolysis of low-rank coal in different ways. These studies show that calcium-containing compounds can change the pyrolysis reaction path of coal, effectively regulate the composition of pyrolysis products, and optimize the pyrolysis process. Although calcium-containing compounds have a significant impact on tar and pyrolysis gas, existing research has rarely explored the inhibitory effect on the release of corrosive elements such as Na and Cl. In addition, these additives form residues after pyrolysis that still need to be disposed of, which can have adverse effects on the environment and increase costs. This study used phosphorite as an additive, which differs from studies of these calcium-based compounds. Phosphorite can be directly recycled after pyrolysis with coal and used in the process of thermal phosphoric acid, which solves the post-processing problem of traditional additives. This not only reduces the difficulty of processing industrial solid waste, but also improves the recycling efficiency of resources. Moreover, in addition to affecting the properties of tar and char, phosphorite can also significantly reduce the release of Na and Cl in coal pyrolysis. The release of Na and Cl is the main cause of equipment corrosion and scaling. Phosphorite can form stable compounds with these elements in coal to inhibit their volatilization and reduce the risk of equipment corrosion. Therefore, this study provides a more efficient and environmentally friendly pyrolysis additive that can enhance the industrial application prospects and utilization value of high-alkali low-rank coal.

Fig. 14 shows the mechanism of low-order and high-alkali coal co-pyrolysis with phosphorite. Following processing, low-rank coal is combined with phosphorite and subjected to pyrolysis in a fluidized bed reactor. During the pyrolysis process, the calcium-containing compounds in phosphorite react with functional groups such as carboxyl and hydroxyl groups in coal, acting as cross-linking points that immobilize some of the large molecular fragments. This process impedes the cracking of char into smaller tar molecules, increasing the yield of char. The calcium-containing compounds also catalyze the cracking of polycyclic aromatic hydrocarbons in tar and facilitate the cleavage of phenols and hydroxyl groups, resulting in lighter tar products during pyrolysis. Moreover, these calcium-containing compounds promote the detachment of methyl and other side chains from aromatic rings in coal, leading to the generation of H_2 and the dealkylation of aromatic components to form CH_4, significantly enhancing the gas yield. Compounds containing sodium and chlorine released during pyrolysis of coal react with the components in phosphorite. NaCl will react with SiO_2, Al_2O_3, CaO and other substances to form relatively stable compounds such as $NaAlSi_3O_8$ and $Na_2Ca_3Si_6O_{16}$ that remain in the solid phase. HCl will react with Al_2O_3, CaO, MgO and other substances to generate compounds such as $Na_3Mg(CO_3)_2Cl$, $AlCl_3$ and $CaCl_2$ with higher melting points. These reactions effectively reduce the release of corrosive

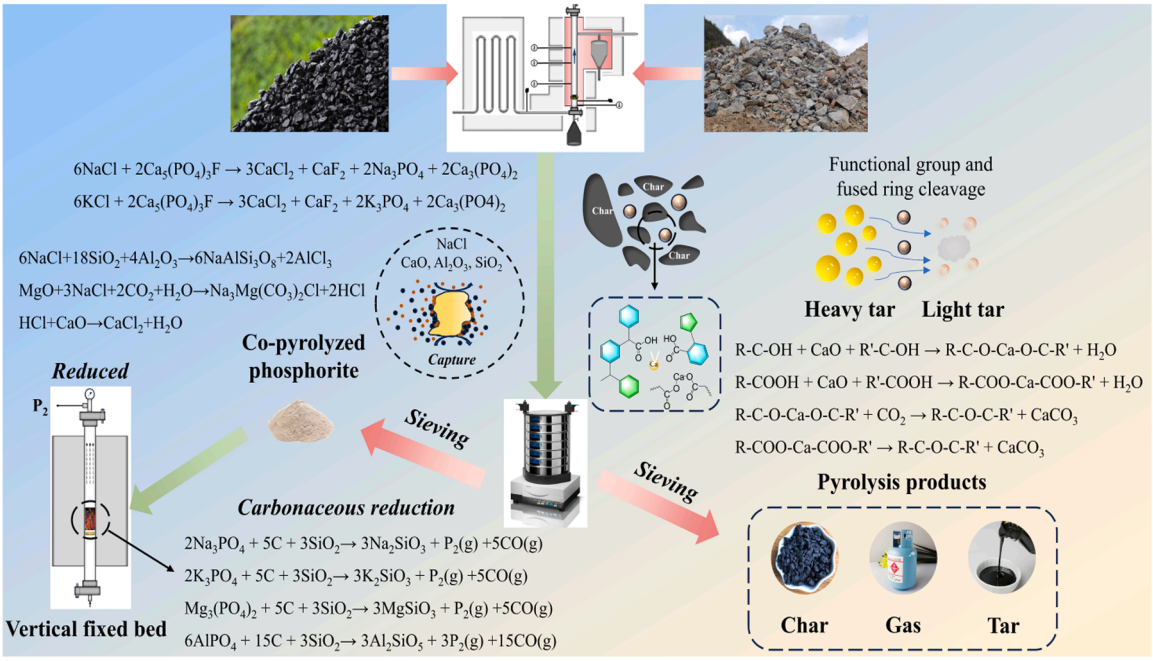

Fig. 14. Mechanism diagram of low-order and high-alkali coal pyrolysis with phosphorite.

chlorides. This is crucial for industrial applications. In high-temperature environments, especially in pyrolysis gas atmospheres, compounds containing sodium and chlorine can cause serious corrosion to equipment, shorten equipment life and increase maintenance costs[93,94]. The formation of substances such as $NaAlSi_3O_8$ and $Na_2Ca_3Si_6O_{16}$ captures these corrosive compounds and converts them into more stable solid products, avoiding their release into the gas phase. This not only reduces the frequency of shutdown maintenance, but also makes the pyrolysis of high-alkali coal safer and more sustainable in industrial applications, improving the utilization value of high-alkali and low-rank coal. In addition, during co-pyrolysis, phosphorite reacts at high temperatures with substances such as MgO, NaCl, and KCl in high-alkali coal, producing Na_3PO_4, K_3PO_4, and $Mg_3(PO_4)_2$, which are more readily reducible by carbon. The recovery and utilization of phosphorite involved in pyrolysis process significantly improve the conversion efficiency, thereby reducing production costs and enhancing the overall efficiency of producing high-purity phosphorus chemicals.

4. Conclusion

This study investigated the synergistic effect of co-pyrolysis of phosphorite and high-alkali and low-rank coal, enhancing the extraction of high-value chemicals like tar while improving coal utilization. The method supports clean and efficient coal use, aligns with China's energy conservation and emission reduction policies, and reduces the release of corrosive substances during coal combustion, ensuring stable operation of coal-fired power plants. It also utilizes China's abundant high-alkali coal, contributing to energy security and reducing reliance on imports. Moreover, it promotes efficient phosphorite utilization, lowering costs in phosphorus chemical production. Overall, this method advances clean coal utilization and aligns with China's sustainable development goals. The main conclusions are summarized as follows.

(1) **Effect on pyrolysis products:** Phosphorite promotes the breakage or substitution of the macromolecular structure in coal. The experimental results show that after co-pyrolysis with phosphorite, the char yield of NM coal at 700 °C increased by 3.14 %, the pyrolysis gas yield increased by 0.65 %, the pyrolysis water yield increased by 0.51 %, and the tar yield decreased by 5.29 %. The changes in the products of co-pyrolysis of HM coal and phosphorite are consistent with those of NM coal.

(2) **Characterization of Pyrolysis Products:** Phosphorite promotes the conversion of long-chain tar into short-chain carbon molecules and decomposes polycyclic aromatic hydrocarbons into monocyclic aromatic hydrocarbons or other small molecules. At 800 °C, the co-pyrolysis of NM coal and Phosphorite can reduce the PH proportion in tar from 29.16 % to 12.50 %, while the contents of CH_4 and H_2 increase by 10.1 $mg \bullet g^{-1}$ and 23.0 $mg \bullet g^{-1}$. This improves the tar quality, significantly increases the combustible gas content in the pyrolysis gas, and increases the utilization value of the pyrolysis products.

(3) **Reduction of Corrosive Substances:** Phosphorite will react with NaCl and other components in the coal to produce high-melting-point sodium calcium silicate, sodium aluminum silicate and other substances. At 900 °C, after adding phosphorite, the release of Na and Cl during the pyrolysis of NM coal decreased by 15.67 % and 16.05 % respectively. This can effectively inhibit the release of corrosive substances and ensure the safe and stable operation of the pyrolysis equipment.

(4) **Conversion ratio of phosphorite:** After co-pyrolysis, the thermal reduction conversion ratio of phosphorite is significantly improved, and the activation energy of the reaction system is reduced by 27.965 kJ/mol, indicating that co-pyrolysis not only accelerates the reaction process, but also enhances the conversion ratio of phosphorite.

Funding

Thanks for the financial supported by the Fundamental Research Funds for the Central Universities (2022ZFJH004).

CRediT authorship contribution statement

Xu Guohui: Resources, Project administration. **Jia Ruiqing:** Writing – review & editing, Formal analysis. **Deng Qigang:** Resources, Project administration. **Ma Dong:** Writing – review & editing, Software. **Chen Yingchi:** Writing – review & editing. **Zhang Bin:** Writing – review & editing, Methodology, Formal analysis. **Wang Qinhui:** Writing – review

& editing, Visualization, Project administration, Methodology, Investigation, Data curation. **Tian Zhihua:** Writing – review & editing, Writing – original draft, Software, Methodology, Investigation, Formal analysis, Data curation.

Declaration of Competing Interest

The authors declare that they have no known competing financial interests or personal relationships that could have appeared to influence the work reported in this paper.

Acknowledgments

Thanks for the technical and financial supported by Dongfang Electric Corporation-Zhejiang University Joint Innovation Research Institute. Thanks for the financial supported by the Fundamental Research Funds for the Central Universities (2022ZFJH004).

Appendix A. Supporting information

Supplementary data associated with this article can be found in the online version at doi:10.1016/j.jece.2025.115559.

Data availability

Data will be made available on request.

References

[1] W. Chen, C. Wang, D. Wei, et al., Influences of salic mineral additives on release and migration of Na/Ca/Fe during O_2/CO_2 combustion of zhundong coals. Adv. N. Renew. Energy 5 (1) (2017) 16–22.
[2] J. Si, X. Liu, M. Xu, et al., Effect of kaolin additive on PM2.5 reduction during pulverized coal combustion: importance of sodium and its occurrence in coal, Appl. Energy 114 (2014) 434–444.
[3] E. Guo, G. Wang, J. Chen, et al., Products characteristics and char gasification reactivity of Naomaohu coal hydropyrolysis, Clean. Coal Technol. 30 (4) (2024) 1–9.
[4] L. Dai, N. Zhou, Y. Lv, et al., Pyrolysis technology for plastic waste recycling: a state-of-the-art review, Prog. Energy Combust. Sci. 93 (2022) 101021.
[5] A. Aisha, S. Muhammad, M. Gordon, et al., A review of pyrolysis technologies and feedstock: a blending approach for plastic and biomass towards optimum biochar yield, Renew. Sustain. Energy Rev. 167 (2022) 112715.
[6] Y. Zhao, J. Yuan, S. Zhao, et al., Is pyrolysis technology an advisable choice for municipal solid waste treatment from a low carbon perspective, Chem. Eng. J. 449 (2022) 137785.
[7] Z. Liu, Advancement in coal chemistry: structure and reactivity, Sci. Sin. Chim. 44 (09) (2014) 1431–1439.
[8] P.P. Sripada, T. Xu, M.A. Kibria, et al., Comparison of entrained flow gasification behaviour of Victorian brown coal and biomass, Fuel 203 (2017) 942–953.
[9] C. Zhu, S. Qu, J. Zhang, et al., Distribution, occurrence and leaching dynamic behavior of sodium in Zhundong coal, Fuel 190 (2017) 189–197.
[10] A. Muhammad, E. Dina, M.B. Muneer, et al., Efficient electrochemical conversion of CO_2 into formic acid using colloidal NiCo@rGO catalyst, Results Eng. 21 (2024) 101824.
[11] A. Muhammad, E. Dina, M. Nafis, et al., Enhanced electrochemical conversion of CO_2 into formic acid using $PbSO_4$/AtSn electrode: catalyst synthesis and process optimization, J. Environ. Chem. Eng. 11 (6) (2023) 111352.
[12] A. Muhammad, A. Azka, T. Chen, et al., Development of PANI/BN-based absorbents for water remediation, Water Qual. Res. J. 54 (4) (2019) 290–298.
[13] J. Zhang, C. Han, Z. Yan, et al., The varying characterization of alkali metals (Na, K) from coal during the initial stage of coal combustion, Energy Fuels 15 (4) (2001) 786–793.
[14] S. Kyi, B.L. Chadwick, Screening of potential mineral additives for use as fouling preventatives in Victorian brown coal combustion, Fuel 78 (1999) 845–855.
[15] X. Qi, G. Song, S. Yang, et al., Migration and transformation of sodium and chlorine in high-sodium high-chlorine Xinjiang lignite during circulating fluidized bed combustion, J. Energy Inst. 92 (3) (2019) 673–681.
[16] X. Zeng, Y. Wang, J. Yu, et al., Coal pyrolysis in a fluidized bed for adapting to a two-stage gasification process, Energy Fuels 25 (3) (2011) 1092–1098.
[17] F. Xue, D. Li, Y. Guo, et al., Technical progress and the prospect of low-rank coal pyrolysis in China, Energy Technol. 5 (11) (2017) 1897–1907.
[18] T. Lv, C. Zhang, C. Wu, Study on the effect og coal diameter and heating rate on the coal pyrolysis, Coal Convers. 28 (1) (2005) 17–20.
[19] G. Jon, K. Rafael, Coal pyrolysis yields from fast and slow heating in a wire-mesh apparatus with a gas sweep, Energy Fuels 2 (4) (1988) 505–511.
[20] W. Chun, W.A. Scaroni, R.G. Jenkins, Effect of pressure on the devolatilization and swelling behavior of a softening coal during rapid heating, Fuel 70 (8) (1991) 957–965.
[21] W. Xu, T. Akira, Effect of coal type on the flash pyrolysis of various coal, Fuel 66 (5) (1987) 627–631.
[22] L. Cui, W. Lin, J. Yao, Influences of temperature and coal particle size on the flash pyrolysis of coal in a fast-entrained bed, Chem. J. Chin. Univ. 22 (1) (2006) 103–110.
[23] C. Ma, Y. Zhao, T. Lang, et al., Pyrolysis characteristics of low-rank coal in a low-nitrogen pyrolysis atmosphere and properties of the prepared chars, Energy 277 (4) (2023) 127524.
[24] N. Wang, Y. Huang, Q. Liu, et al., Effects of pyrolysis conditions on pressurized pyrolysis of xiwan coal in fluidized bed, Coal Convers. 44 (6) (2021) 34–43.
[25] T. Liu, J. Zhao, X. Zhang, Directional Conversion of Volatiles from Low-Rank Coal to BTX-Rich Tar by Combined *In Situ* and *Ex Situ* Catalytic Pyrolyses, ACS Omega 8 (4) (2023) 4419–4428.
[26] Y. Ban, L. Jin, K. Wang, et al., Catalytic effect of industrial waste carbide slag on pyrolysis of low-rank coal[J], Energy 265 (2023) 126368.
[27] N.A. Öztaş, Y. Yürüm, Pyrolysis of Turkish Zonguldak bituminous coal. Part 1. Effect of mineral matter, Fuel 79 (10) (2000) 1221–1227.
[28] J. Yang, N. Cai, A TG-FTIR study on catalytic pyrolysis of coal. J. Fuel Chem. Technol. 34 (6) (2006) 650–654.
[29] H.D. Franklin, W.A. Peters, J.B. Howard, Mineral matter effects on the rapid pyrolysis and hydropyrolysis of a bituminous coal: 2. Effects of yields of C_3-C_8 hydrocarbons, Fuel 61 (12) (1982) 1213–1217.
[30] Y. Wu, Q. Zhang, J. Zhuo, et al., Influence of calcium chloride on the fine particulate matter formation during coal pyrolysis, Fuel 355 (8) (2023).
[31] H.D. Franklin, W.A. Peters, J.B. Howard. Mineral matter effects on the rapid pyrolysis and hydropyrolysis of a bituminous coal. 1. Effects on yields of char, tar and light gaseous volatiles[J]. 1982, 61(2): 155-160.
[32] M. Kenji, S. Hiroyuki, O.J. Ichi, et al., Effects of metal ions on the thermal decomposition of brown coal, Fuel Process. Technol. 46 (3) (1996) 183–194.
[33] R. Cao, Y. Li, J. Xia, et al., $NiSO_4$ as additive effect on the carbothermal reduction process of phosphorite rock and SiO_2, Silicon 1 (2019) 1–8.
[34] R. Geng, J. Xia, Z. Chen, et al., Effects of potassium feldspar on slagging and fluxing in phosphorus produced via electric furnace, Phosphorus Sulfur Silicon Relat. Elem. 192 (4) (2017) 475–480.
[35] Y. Li, Z. Chen, R. Geng, et al., Studies on extraction of phosphorus ore by electric furnace with different fluxing agents, Phosphorus Sulfur Silicon Relat. Elem. 193 (3) (2018) 141–148.
[36] R. Kijkowska, Z. Kowalski, D. Pawlowska-Kozinska, et al., Tripolyphosphorite made from wet-process phosphoric acid with the use of a rotary kiln, Ind. Eng. Chem. Res. 47 (18) (2008) 6821–6827.
[37] R. Kijkowska, D. Pawlowska-Kozinska, Z. Kowalski, et al., Wet-process phosphoric acid obtained from Kola apatite. Purification from sulphates, fluorine, and metals, Sep. Purif. Technol. 28 (3) (2002) 197–205.
[38] P. Wu, L. Lv, S. Tang, et al., The fouling properties of SiO_2–CaO–P_2O_5 system in high-temperature rotary kiln phosphoric acid process, Chin. J. Chem. Eng. 28 (7) (2020) 1824–1831.
[39] B. Deng, Experimental Study on the Effect of Ca-based Additives on Pyrolysis and Combustion Characteristics of Bituminous Coal, Changsha University of Science & Technology, 2020.
[40] R. Zhang, Experiments on sulfur transformation during coal pyrolysis combined with production of tar char and gas in double fluidized bed, Zhejiang University, 2021.
[41] M. Siyiti, Experimental research on the influence of atmosphere on pyrolysis characteristic during coal pyrolysis in fluidized bed reactor, Zhejiang University, 2018.
[42] K. Li, Research on coal pyrolysis-based technology co-producing tar char gas in dual fluidized beds with char heat carrier. Zhejiang University, 2022.
[43] Z. Tian, Q. Wang, D. Ma, et al., Effect of aluminium sulfate on carbothermal reduction of phosphorite in a fluidized bed, J. Ind. Eng. Chem. 139 (2024) 138–148.
[44] G. Zheng, R. Cao, Y. Li, et al., The Additive Effect of K_2CO_3-$NiSO_4$ on the Carbothermal Reduction Process of Phosphorite Rock and SiO_2, Silicon 12 (2019) 1985–1994.
[45] X. Wei, J. Huang, T. Liu, et al., Transformation of alkali metals during pyrolysis and gasification of a lignite, Energy Fuels 22 (3) (2008) 1840–1844.
[46] Y. Jia, J. Huang, Z. Cheng, et al., Effect of CaO on tar cracking in a rapid-pyrolysis fixed bed reactor, Coal Convers. 24 (2) (2011) 53–57.
[47] Y. Xiong, Q. Wang, Y. Yang, et al., Experimental study on influence of calcium carbonate on coal pyrolysis behaviors, Therm. Power Gener. 45 (1) (2016) 14–19.
[48] X. Li, J. Cen, Z. Xia, et al., Pressurized pyrolysis characteristics of pine sawdust and coal, J. Zhejiang Univ. Eng. Sci. 53 (7) (2019) 1298–1305.
[49] F. Mushtaq, R. Mat, F.N. Ani, Fuel production from microwave assisted pyrolysis of coal with carbon surfaces, Energy Convers. Manag. 110 (15) (2016) 142–153.
[50] W. Duan, Q. Yu, H. Xie, et al., Pyrolysis of coal by solid heat carrier-experimental study and kinetic modeling, Energy 135 (15) (2017) 317–326.
[51] R. Ebrahimi-Kahrizsangi, M.H. Abbasi, Evaluation of reliability of Coats-Redfern method for kinetic analysis of non-isothermal TGA, Trans. Nonferrous Met. Soc. China 18 (1) (2008) 217–221.
[52] S.Y. Yorulmaz, A.T. Atimtay, Investigation of combustion kinetics of treated and untreated waste wood samples with thermogravimetric analysis, Fuel Process. Technol. 90 (7) (2009) 939–946.
[53] J. Wang, M. Fang, Z. Luo, et al., Research on fast thermolysis kinetics of coal, Proc. CSEE 27 (17) (2007) 18–22.

[54] M. Li, Studies on Coal Catalytic Pyrolysis Characteristics during Hydrogen-rich Atmosphere[D], Zhejiang University, 2015.
[55] S. Wang, Q. Sun, X. Hu, et al., Fissure evolution and variation of pyrolysis kinetics parameters of tar-rich coal during heat treatment under different atmosphere, Coal Sci. Technol. 52 (1) (2024) 15–24.
[56] Q. Sun, W. Li, H. Chen, et al., The variation of structural characteristics of macerals during pyrolysis, Fuel 82 (6) (2003) 669–676.
[57] P.R. Solomon, D.G. Hamblen, R.M. Carangelo, et al., Models of tar formation during coal devolatilization, Combust. Flame 71 (2) (1988) 137–146.
[58] T. Zhu, S. Zhang, J. Huang, et al., Effect of calcium oxide on pyrolysis of coal in a fluidized bed, Fuel Process. Technol. 64 (3) (2000) 271–284.
[59] J. Zhang, J. Li, Y. Mao, et al., Effect of $CaCO_3$ addition on ash sintering behaviour during K_2CO_3 catalysed steam gasification of a Chinese lignite, Appl. Therm. Eng. 111 (2017) 503–509.
[60] O. Yasuo, A. Kenji, Ion-exchanged calcium from calcium carbonate and low-rank coals: high catalytic activity in steam gasification, Energy Fuels 10 (2) (1996) 431–435.
[61] L. Zhang, S. Kudo, N. Tsubouchi, et al., Catalytic effects of Na and Ca from inexpensive materials on in-situ steam gasification of char from rapid pyrolysis of low rank coal in a drop-tube reactor, Fuel Process. Technol. 113 (2013) 1–7.
[62] L.R. Radović, P.L. Walker Jr., R.G. Jenkins, Effect of lignite pyrolysis conditions on calcium oxide dispersion and subsequent char reactivity. Fuel 62 (2) (1983) 209–212.
[63] P. Liu, D. Zhang, L. Wang, et al., The structure and pyrolysis product distribution of lignite from different sedimentary environment, Appl. Energy 163 (2016) 254–262.
[64] D. Hu, Z. Li, Y. Liu, et al., Coal pyrolysis law and mechanism of index gas generation in Linsheng Mine, J. Mol. Struct. 1297 (1) (2024) 136912.
[65] W. He, Z. Liu, Q. Liu, et al., Behaviors of radical fragments in tar generated from pyrolysis of 4 coals, Fuel 134 (2014) 375–380.
[66] S. Lin, H. Michiaki, S. Yoshizo, et al., Comparison of pyrolysis products between coal, coal/CaO, and coal/$Ca(OH)_2$ materials, Energy Fuels 17 (3) (2003) 602–607.
[67] D.L. Ellig, C.K. Lai, D.W. Mead, et al., Pyrolysis of volatile aromatic hydrocarbons and n-heptane over calcium oxide and quartz, Ind. Eng. Chem. Process Des. Dev. 24 (4) (1985) 1080–1087.
[68] C.S. Lai, P. Chen, J.P. Longwell, et al., Thermal reactions of m-cresol over calcium oxide between 350 and 600 ℃, Fuel 66 (4) (1987) 525–531.
[69] H. Yin, M. Wang, J. Wang, et al., Effect of calcium and sodium additives on the pyrolysis characteristics of Pingshuo demineralized coal, Clean. Coal Technol. 3 (2010) 31–35.
[70] J. Yang, N. Cai, Y. Zhang, et al., Experimental study for the effect of catalystson the release of gaseous products during pyrolysis of lignite, J. Eng. Thermophys. 30 (1) (2009) 161–164.
[71] L. Xu, H. Liu, D. Zhao, et al., Transformation mechanism of sodium during pyrolysis of Zhundong coal, Fuel 233 (2018) 29–36.
[72] T. Zhu, S. Zhang, J. Huang, et al., Effect of calcium oxide on pyrolysis of coal in a fluidized bed, Fuel Process. Technol. 64 (1) (2000) 271–284.
[73] C.C. Cheng-Shiou, Thermal reactions of freshly generated coaltar over calcium oxide[D], Massachusetts Institute of Technology, Cambridge, USA, 1986.
[74] L. Zhang, S. Hu, Q. Chen, Molecular structure characterization of the tetrahydrofuran-microwave-extracted portions from three Chinese low-rank coals, Fuel 189 (1) (2017) 178–185.
[75] R. Lin, G.P. Ritz, Studying individual macerals using i.r. micro-spectrometry and implications on oil versus gas/condensate proneness and “low-rank” generation, Org. Geochem. 20 (6) (1993) 695–706.
[76] H. Li, S. Shi, B. Lin, Effects of microwave-assisted pyrolysis on the microstructure of bituminous coals, Energy 187 (15) (2019) 115986.
[77] K. Wang, J. Ding, J. Deng, et al., Hydrogen generation mechanism of oil-rich coal oxidation in low temperature, Energy 293 (15) (2024) 130739.
[78] A. Azka, A. Muhammad, Q. Sheng, et al., Rational design of highly efficient one-pot synthesis of ternary PtNiCo/FTO nano catalyst for hydroquinone and catechol sensing, Electroanalysis 33 (1) (2021) 170–180.
[79] A. Azka, A. Muhammad, Q. Sheng, et al., A non-enzymatic hydrogen peroxide sensor with enhanced sensitivity based on Pt nanoparticles, Anal. Sci. 37 (2021) 1419–1426.
[80] X. Li, Research mechanism of vacuum carbothermic reduction of $Ca_3(PO_4)_2$ with three exogenous additives, Guizhou University, 2022.
[81] L. Mu, Analysis of element migration and variation during carbothermal reduction of phosphorites and residue features after reaction, Kunming University of Science and Technology, 2021.
[82] B. Hu, C. Ma, K. Gui, et al., Effect of inorganic additives on smelting reduction of phosphorite rock, Ind. Miner. Process. 06 (2014). : 1-2+ 8.
[83] R. Cao, Basic research on the influence of dopants on carbothermic reduction of phosphorite rock, Kunming University of Science and Technology, 2019.
[84] D.W. Mckee, C.L. Spiro, P.G. Kosky, et al., Catalysis of coal char gasification by alkali metal salts, Fuel 62 (2) (1983) 217–220.
[85] W. Shen, L. Xiong, X. Sha, Formation and removal of gaseous alkali metal of hot gas, Gas. Heat. 18 (6) (1998) 3–5.
[86] M.R. Khan, K. Seshadri, Compositional changes in the mild gasification liquids produced in the presence of calcium compounds, Fuel Process. Technol. 27 (1) (1991) 83–94.
[87] N. Tsubouchi, C.C. Xu, Y. Ohtsuka, Carbon crystallization during high-temperature pyrolysis of coals and the enhancement by calcium, Energy Fuels 17 (5) (2003) 1119–1125.
[88] Y. Jia, J. Huang, Y. Wang, Effects of calcium oxide on the cracking of coal tar in the freeboard of a fluidized bed, Energy Fuels 18 (6) (2004) 1625–1632.
[89] X. Zou, J. Yao, X. Yang, et al., Catalytic effects of metal chlorides on the pyrolysis of lignite, Energy Fuels 21 (2) (2007) 619–624.
[90] H. Liu, J. Zhou, J. Wang, Effects of Ca-based additives on behaviors of slow and fast coal pyrolysis, Mod. Chem. Ind. 31 (3) (2011) 70–72.
[91] L. Liu, H. Liu, M. Cui, et al., Calcium-promoted catalytic activity of potassium carbonate for steam gasification of coal char: transformations of sulfur, Fuel 112 (2013) 687–694.
[92] Y. Ban, L. Jin, J. Zhu, et al., Insights into effect of $Ca(OH)_2$ on pyrolysis behaviors and products distribution of Hongshaquan coal, Fuel 307 (1) (2022) 121791.
[93] Z. Qu, R. Zhong, L. Wang, et al., Research progress on high temperature corrosion mechanism of waste incineration power generation boiler, IOP Conf. Ser.: Earth Environ. Sci. 598 (2020) 012008.
[94] M.A. Uusitalo, P.M.J. Vuoristo, T.A. Mäntylä, High temperature corrosion of coatings and boiler steels below chlorine-containing salt deposits, Corros. Sci. 46 (6) (2004) 1311–1331.